3D Printing of Soft Hydrogels Incorporating Functional Nanomaterials

by

Yun Wu

A thesis

presented to the University of Waterloo

in fulfillment of the

thesis requirement for the degree of

Master of Science

in

Chemistry (Nanotechnology)

Waterloo, Ontario, Canada, 2016

AUTHOR'S DECLARATION

I hereby declare that I am the sole author of this thesis. This is a true copy of the thesis, including any required final revisions, as accepted by my examiners.

I understand that my thesis may be made electronically available to the public.

Abstract

Tissue engineering (TE) scaffolds are required to closely mimic the human body environment to enable the study of cell behavior *in vitro* and allow the fabrication of artificial tissue constructs. The scaffolds should possess controlled structural and mechanical properties, such as stiffness and porosity. In addition, its physical and chemical properties, such as electrical conductivity, should be able to promote cell differentiation and growth. In the search of developing an ideal scaffold, hydrogels that incorporate functional nanomaterials scaffolds are being explored.

This study, as a fulfillment for a master's degree, investigates the ability of cells to survive in a three-dimensional (3D) printed soft hydrogels incorporated with functional materials. In this work, alginate, a natural polymer, was used as the main hydrogel material. It can physically crosslink by adding $CaCl_2$ or chemically crosslink after methacrylation, by introducing carbon-carbon double bonds. However, pure alginate hydrogel is mechanically and rheologically weak. Previous mechanical tests indicated that cellulose nanocrystals (CNC)-incorporated alginate-based hydrogels increased the mechanical strength of the scaffolds, which can contribute to the interactions between CNC and polymeric networks. Rheological tests showed that the incorporation of cellulose nanocrystals into the alginate matrix introduced strong shear thinning behavior and improved shear modulus. The enhancement of rheological properties improved the printability and fidelity of the hybrid pre-gel solution. Finally, cell viability was explored by suspending 3T3 fibroblasts in the bioink. It was shown that the hybrid bioink was nontoxic and the cell viability remained high over a 7-days period.

This master's thesis demonstrates the feasibility of 3D printing of soft hydrogels for the fabrication of 3D scaffolds that mimic real tissues. It is anticipated that a broad array of ink compositions with suitable viscosity can be printed and multiple cell lines can grow in the same scaffold. This research provides a platform for the fabrication of biocompatible polymers and stretchable biosensors within an engineered scaffold.

Acknowledgements

I would like to thank my supervisor Dr. Shirley Tang for her great help in my research and studies. She really did help me a lot through discussions.

I would like to thank my committee members, Prof. Xiaosong Wang and Prof. Michael Tam for their feedback and suggestions on my thesis, and for their guidance during my master study.

I would like to thank Prof. Hyock Ju Kwon's, Prof. Michael Tam's, and Prof. Juewen Liu's group for providing access to the compression tester, rheometer, and fluorescence microscope, respectively.

I would like to thank the past and current group fellows: Mike Coleman, Zhi Li, Kai Wang, Gaganprit Gill, Andrew Wenger, and especially Louis Cheung and Irfani Ausri who offered kind help to me. They provided me with technical guidance and knowledge in the lab.

I would like to thank Dr. Zengqian Shi, Debbie Wu, Yibo Liu, and Jimmy Huang for their providing information on materials characterization and instruments training.

I would like to thank my parents for supporting my master studies.

Table of Contents

List of Figures

List of Tables

List of Abbreviations

2D: two-dimensional

3D: three-dimensional

ACPs: amorphous calcium phosphates

AEMA: 2-aminoethyl methacrylate

ALG-CNC: alginate-cellulose nanocrystals

BCPs: biphasic calcium phosphates

CAD: computer-assisted design

CNC: cellulose nanocrystal

CNT: carbon nanotubes

CPCs: calcium phosphate ceramics

CT: computed tomography

DIW: direct ink writing

DMEM: Dulbecco's Modified Eagle's Medium

ECM: extracellular matrix

EDC: 1-ethyl-3-(3-dimethylaminopropyl)-carbodiimide hydrochloride

FBS: fetal bovine serum

FDA: Food and Drug Administration

FDM: fused deposition modeling

GAG: glycosaminolglycan

GelMA: gelatin methacrylate

GO: graphene oxide

HA: hyaluronic acid

HAP: hydroxyapatite

hMSCs: human mesenchymal stem cells

HNDFs: human neonatal dermal fibroblasts

HUVEC: human umbilical vein endothelial cell

ICPs: intrinsically conductive polymers

IR: infrared

LVR: linear viscoelastic region

MA: methacrylate

MAALG: methacrylated alginate

MES: 2-morpholinoethanesulfonic acid

MRI: magnetic resonance imaging

NHS: N-hydroxylsuccinimide

NMR: nuclear magnetic resonance

PANI: polyaniline

PB: particle binding

PEG: poly (ethylene glycol)

PEI: poly (ethylenimine)

PEO: poly (ethylene oxide)

pHEMA: poly (2-hyroxyethyl methacrylate)

PPE: poly (p-phenylene ethylene)

PPO: poly (propylene)

PPy: polypyrrole

RGD: Arg-Gly-Asp

SEM: scanning electron microscopy

SLA: stereolithography

SLS: selective laser sintering

SPH: super-porous hydrogels

STL: standard tessellation language

TCP: tricalcium phosphate

TE: tissue engineering

T_g: glass transition temperature

µ-SLA: micro SLA

UV: ultraviolet

Chapter 1. Introduction

1.1 3D Printing

3D printing, which is also known as additive manufacturing, is a term used to describe a process that fabricates a 3D object layer-by-layer where each new layer is deposited on the previously formed one. 3D printers are seamlessly integrated with a computer-assisted design (CAD) software. The designed patterns are saved as standard tessellation language (STL) files and then converted to G-codes that are readable by the 3D printers.[1,2] There are several advantages of 3D printing over traditional manufacturing process.[3] Firstly, custom products can be produced cheaper and faster. Secondly, it does not require milling nor producing scraps because the excess materials can often be recycled. Thirdly, it allows the products to be designed in-house and the designs may be easily shared. In addition, finely-structured objects can also be readily produced in large quantities through 3D printing technology.

In 3D printing, a wide range of raw materials, such as plastics, resins, super alloys, stainless steel, polymers and ceramics, can be used.[3,4] In order to precisely print an object there are many factors that need to be considered, including the material's strength, viscosity, stability, resistance to heat and moisture, and its colour durability.[3]

3D printing technology enables the fabrication of artificial scaffolds based on tissue images scientifically designed or captured with common medical imaging techniques such as computed tomography (CT) and magnetic resonance imaging (MRI).[5] The most common used 3D printing techniques are classified to four different kinds: extrusion-based methods, particle fusion-based methods, light induced methods, and inkjet printing (Figure 1.1).[1,2,5–10]

Extrusion-based printing methods, such as fused deposition modeling (FDM) and direct ink writing (DIW), are widely used to fabricate devices or scaffolds for tissue engineering (TE). The extrusion-based printing technique is based on the technique where the materials are extruded through a nozzle and a three-axis motion control system is used to control the movement of nozzles to build up complex 3D objects layer-by-layer. In traditional FDM, where plastics is used, a heating system is needed to melt the materials.

Molten systems employ pre-heating chambers and provide a heat source to bring the filaments, typically 1.75 mm in diameter to their melting points. The materials are then extruded under an applied pressure. If the pressure remains constant, the extrusion speed and the cross-sectional diameter of the extruded filaments will also stay constant. The extruded molten materials must solidify quickly to retain their shapes and bind to the existing layers. In the case of plastics, the molten materials immediately solidify after extrusion due to the decrease in temperature.[4] For DIW in TE, the cell encapsulated materials are extruded through a nozzle driven by a pneumatic or mechanical tool.[5] The bioinks are reserved in a reservoir, like a syringe. Thus, although various bioinks with a wide range of viscosities can be extruded, the hydrogel with higher viscosities are preferred because they are able to retain their shape after extrusion. The resolution of the printed constructs is 200-500 μm as determined by nozzle diameter.[5] One disadvantage of the method is the fabrication of the unsupported sections. It is hard for the materials to support themselves immediately upon extrusion, leading to the spreading or collapse of unsupported segments. Approaches to solve the problem are recently discovered. One method is to introduce the supporting materials during the printing process and then removed after printing. These materials are supposed to be dissolved or burned out easily without destroying the required constructs and dual extruders are needed. In summary, extrusion-based 3D printing is easy to use and have been employed for tissue engineering applications.

Inkjet printing produces small volumes (1-100 picoliters) of droplets from a nozzle to a printing platform. The droplets are generated through electrically heating the nozzle to produce a vapor bubble or breaking the liquid into droplets by piezoelectric actuator.[5,6] There are three important stages in inkjet printing including drop formation, drop/substrate interaction, and drop solidification. At the drop generation stage, the ink's viscosity is the most important property. The viscosity of the ink should be very low usually below 10 mPa s at high shear rates. At the drop-substrate interaction stage, the surface tension is a vital factor because it determines the shape of the droplets after extrusion through the nozzle and on the surface of the substrate. The general value of surface tension is in the range of 28-350 mN m^{-1}. The two phase interactions accompanied by the drop solidification control the final shape and size of the printed objects. The spatial resolution of inkjet printing is determined by the interaction between adjacent droplets and

between droplets and the substrate.[6]

Particle fusion printing methods, consisting of selective laser sintering (SLS) and particle binding (PB), can be used to print complex constructs made of polymers, ceramics, metals and composites. A directed laser beam is used to raise the temperature of the polymers or metal particles over their melting points to fuse the particles together. The beam is moved over the cross section of the designed model to create a single layer, where a new layer of particles are dispensed on the top. The process is then repeated until finishing the desired constructs. The materials suitable for SLS are powder with a size ranging from 10 to 100 μm, having an attainable melting point and capable of binding together when heated. In addition, due to the fine particle flow dynamics in the bed system functionalized surface is required to eliminate electrostatic forces.[5] PB has the same principle as SLS except for the laser induced melting of particles. A liquid binding solution is used to fuse particles together within each layer and the final 3D objects are solidified by a high-temperature sinter procedure. The resolution of the method, affected by the particle size, particle size distribution, material binding properties, and laser or binder width, is in the range of 700 to 1000 μm horizontally and 100 μm vertically.[5]

Light induced 3D printing, also known as stereolithography (SLA), is the oldest 3D printing technique, developed in the 1980s.[5–7] SLA enables the solidification of the liquid polymers by ultraviolet (UV), infrared (IR), or visible light. The viscosities of the polymer liquid vary from 1 mPa s to 300 mPa s. After the polymerization of each layer, the platform lowers into the solution to allow the liquid polymer to cover the printed surfaces and polymerize on the top of the previous layers. The step height of the platform is typically smaller than the curing depth. Recent developments in light source and refined mirror-lens system have improved the resolution and speed of SLA crosslinking. Tumbleston et al. demonstrated the generation of polymer models up to tens of centimeters in size with the resolution below 100 μm within a few minutes.[11] The smallest resolutions of traditional SLA is approximately 25 μm, whereas micro SLA (μ-SLA) and high-definition SLA are in the single micrometer range. However, the most commonly used UV light beam has limited applications in tissue engineering. In addition, there are only limited suitable biocompatible and biodegradable materials for SLA. Therefore, future efforts will be mainly devoted to the

development of polymer biodegradability, as well as higher-resolution machines.[5]

Overall, DIW, inkjet printing and light induced 3D printing are the techniques suitable for cell printing. DIW method can be utilized to print large constructs in the cm range. It is also suitable in scale-up production and without geometrical limits. However, it has the lowest printing resolution at 100 µm compared to other methods. Inkjet printing is the least technologically complex and expensive methods of cell printers. One of the advantages of inkjet printing is the non-contact to avoid deformation of the printed patterns. It has been shown that the resolution can reach up to 85-300 µm depending on the nozzle sizes. However, the high shear forces applied may cause damage to the cells and the printing of large constructs decreases the cell viability. Light-induced 3D printing is the only orifice-free techniques among the three methods. The advantage of this method is its ability to utilize bioinks with any viscosity and print cells densely at the high resolution of 10 µm to 100 µm. However, the bioinks and photoinitiators have to be carefully considered because only photosensitive pre-gel solution can be used for this method, and cells inside the bioinks may be killed by the UV light and intermediate free radicals. Moreover, it lacks the ability to print multiple types of cells. Depending on their biological applications, a combination of multiple bioprinting methods may be used.

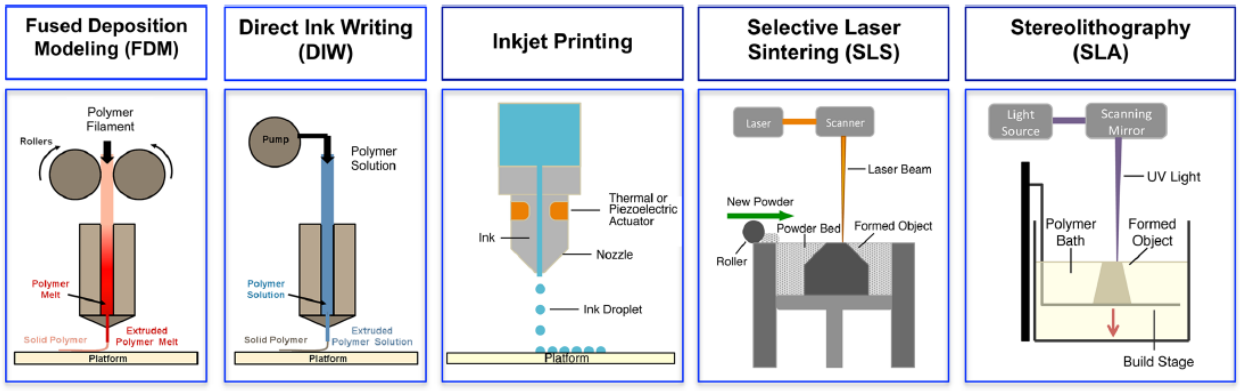

Figure 1.1: Schematics of 3D printing techniques: fused deposition modeling (FDM) and direct ink writing (DIW), inkjet printing, selective laser sintering (SLS), and stereolithography (SLA) (from left to right).[5]

1.2 Tissue Engineering Scaffold

TE is a multidisciplinary and interdisciplinary field of biological science and engineering.[12–14] The purpose of tissue engineering is to overcome the limitations of traditional treatments for patients with organ

complications.[12] In tissue engineering, cells are first isolated from a patient and then allowed to proliferate, migrate and differentiate in a porous matrix, known as a scaffold, to create an engineered tissue.[12–16] The engineered tissue is then grafted into the patient's body to replace the impaired one. Once an ideal artificial tissue is fabricated, the patient may experience no adverse responses, thus making this approach a safer option for tissue regeration.[12]

Conventional two-dimensional (2D) *in vitro* cell culture systems provide a convenient and rapid platform for biochemical analysis.[17] However, restricted cell mobility generally caused by the lack of fluid in the 2D systems can be overcome by the use of 3D scaffolds. For example, it was shown that cancerous cells behave differently in 3D scaffolds compared to 2D systems. The antibody against the β1-integrin surface receptor changed the cancerous cells growth, by changing its shape and growth pattern, in the 3D model but not in the 2D environment.[18] In addition, the effect of 2D and 3D models on cell adhesion, migration, and epithelial morphogenesis is significant. Researches showed that fibroblasts express different shapes, distributions of transmembrane adhesion proteins, and gene expression levels in 3D model when compared to 2D environment. Therefore, a 3D environment can provide a deeper insight into the cell adhesion and migration mechanism. This can be explained by the interaction between the cells and the tissue and adjacent cells within extracellular matrix (ECM) because a 3D model simulates a physiological environment of real tissues. [19]

The most common way to investigate biological processes and develop therapeutic strategies is through *in vivo* animal models and *in vitro* cell culture platforms but there are some drawbacks. Firstly, it is difficult for the *in vitro* cell culture platforms to achieve the integrated multi-organ responses which are easily produced by *in vivo* models. Secondly, the *in vitro* platforms cannot mimic the complicated cell-to-cell and cell-to-matrix interactions that exist in *in vivo* models. Thirdly, data from animal models do not completely reflect the conditions in human physiology. Lastly, there are ethical concerns.[20]

Overall, the cells are seeded into scaffolds that define the geometry of the target tissue or organs and promote tissue regeneration. Each components in the ECM has their own purposes: for example, the dimers of alpha and beta subunits integrins recognize and bind to ECM proteins to trigger signaling events that

influence gene expression whereas fibrin controls stiffness and resists tension.[21,22] The components of ECM vary with different tissues while specific protein breaks down and reshapes the ECM. The biodegradability and stability of the scaffolds should be investigated to evaluate the time at which cells are able to proliferate and develop into tissue before degradation. It is a great challenge to choose the suitable materials to simulate the tissue generation.

There are several requirements for an ideal 3D tissue scaffold. Firstly, the scaffold needs to have similar physical properties, such as mechanical strength and stiffness, as the targeted organs or tissues of the patient.[12,15,16,23] Different tissues have different intrinsic moduli, for example, brain tissue is soft (0.1-1 kPa), muscle tissue tends to be intermediate (10 kPa), the load-bearing cartilage tissue is stiffer (20-25 kPa), while bone tissue is relatively stiff (100 kPa).[24] Cells apply stresses on their matrices during tissue development, morphogenesis and differentiation, and normal physiological functions. The stiffness of the matrix determines the degree of contraction between cells and matrix and cell migration. The stiffer the matrix is, the more difficult it is for cell to contract it.[21] The quality of the remodified tissue when the cells are exposed to suitable mechanically loaded gels during the maturation process is similar to the original tissue.[25] Researches showed that the behavior of fibroblasts is influenced by matrix stiffness. For example, matrix stiffness influences the time and extent of fibroblast cell contraction, and the limit of wound healing and fibrosis.[21]

Secondly, the scaffold must possess interconnecting pores with controlled porosity and pore distribution,[12,15,16,23] because these facilitate the supply of growth factor, cellular invasion, the transport of oxygen and nutrients, as well as the removal of waste products generated from cell metabolism.[13] Optimal cell invasion occurred in a scaffold with a pore size of 100-300 μm, which is 5-10 times the cell diameters.[8] Smaller pore sizes limit the invasion of cells, whereas larger pores create notch effects and lower the sustainability when forces are applied. In addition, the porous structure should enable the sufficient supply of nutrients and the removal of waste to keep the cells inside alive. Gel properties, such as polymer fraction, polymer size, and crosslinker concentration, determine the gel nanoporous structures. For example, molecules with molecular weights less than 1300 Da and Stokes radii less than 1 nm, such as glucose,

oxygen, and Vitamin B12, can freely diffuse in ionically crosslinked alginate. However, the diffusion rate of high-molecular-weight molecules, such as myoglobin, albumin, and fibrinogen, is decreased when the crosslinker concentration is increased.[26] Different scaffolds show different flow or diffusion mechanisms. Scaffolds made of fibrins allow for nutrients to flow through the pores and diffuse throughout the fibrin, but a calcium phosphate-made-scaffold only allows the nutrients to pass through the pores.[25]

Thirdly, the materials for the tissue engineering scaffold need to be biocompatible, biodegradable, and incapable of releasing toxic agents or initiating an inflammatory response.[12,14,15] Biocompatibility involves a positive and controllable contribution to the biological components of the construct, such as the interaction with endogenous tissues and supporting cellular activities. The degradation kinetics of the materials must be understood to evaluate the scaffold's biodegradability. The degradation rate of the artificial scaffolds has to adapt to the new tissue's reconstruction speed. The decomposition rate of biomaterials can be tuned by modifying the crystal phase, structure, and the proportion of the lactide acid and glycol.[25] Furthermore, the degradation byproducts are also important. They should be nontoxic, easily metabolized, and rapidly removed from the body because toxic products can be detrimental to cell viability and functions. Some large molecular weight polymers can be broken down into oligomers or monomers that can cause inflammation.[10]

Fourthly, materials must have appropriate swelling characteristics. Overly swollen materials may absorb fluid from the surrounding environment while contraction may shrink the pores and affect cell migration and nutrient delivery. Therefore, it is necessary to understand the materials' different swelling and contractile characteristics because it can potentially result in deformation of the final construct if materials of different swelling and contractile properties are used together.[10]

Fifthly, the scaffold should have the appropriate surface functionalities to promote cellular attachment, proliferation and differentiation.[10,12,15,27,28] The migration and proliferation rate is higher on a smooth substrate than on a rough surface. A higher migration rate allows a more homogeneous distribution of the cells in a scaffold. However, it does not mean that higher cell migration rates are an advantage in TE techniques.[25] The introduction of surface ligands to a material can improve cell attachment and proliferation

on the substrate. The well-known Arg-Gly-Asp (RGD) motif found in various ECM proteins including fibronectin, laminin, collagen I, fibrinogen, and vitronectin was investigated as a method to improve cell adhesion to the matrix.[29,30] The 3D environment in a tissue scaffold can also influence the cell shape and differentiation process.[10] For the best cell growth inside a scaffold, the adhesion process is vital since it affects the functional differentiation, matrix production and survival. Furthermore, the charge distribution, the wettability and the surface structure determine the adhesion quality.

Nanofibrous materials provide an excellent environment to simulate the architecture formed by fibrillar ECM proteins.[31] The fibrous ECM proteins possess numerous sites of interactions with cell surface receptors. It is thought that cells respond directly to nanoscale surface features by changing their morphology or activity. It has been shown that a number of cells prefer to align along grooved surfaces.[30] There is a tight connection between the cytoskeleton and the ECM through cell surface receptor, so that cells convert mechanical signals into chemical signals, thus influencing cell functions, such as adhesion, migration, and differentiation.[32] Nanometer scale elements can be introduced into TE scaffolds to act as protein fibers because it provides a realistic environment for the cells to interact with the matrix, similar to the fibrous environment of the natural ECM. In contrast, scaffolds without nanoscale materials present a 2D surface to the cells. If the surface of the matrix is endowed with adhesion ligands, the cells tend to flatten as it adheres and spreads as shown in Fig.1.2.[30]

In addition, the scaffold should have certain conductivity to allow cell communication and signal delivery. Electrical stimulation applied on rats with crush injury to the sciatic nerve has been observed to improve tissue regeneration. Moreover, the contractile behavior of the engineered cardiac tissue with high level expressions of cardiac troponin-I and connexin-43 is improved after electrical stimulation.[33] Conducting polymers, such as polypyrrole (PPy) and polyaniline (PANI), are used to modulate cellular activities and have been observed to improve proliferation and assist neural and cardiac stem cell differentiation.[33,34] Conductive nanomaterials, such as graphene and carbon nanotubes (CNT), possess high conductivity and mechanical strength, thus making them good candidates for tissue engineering. Shin et al. introduced CNT into gelatin methacrylate (GelMA) hydrogels to engineer functional cardiac patches. It has

been suggested that the incorporation of CNT showed advanced electrophysiological functions and improved cell adhesion, organization, and cell-to-cell interaction.[35] The nanowire should be longer than the average of thickness of the hydrogel pore wall to ensure the interaction between the cells from both sides and the enhancement of the electrical signal transmission.[36]

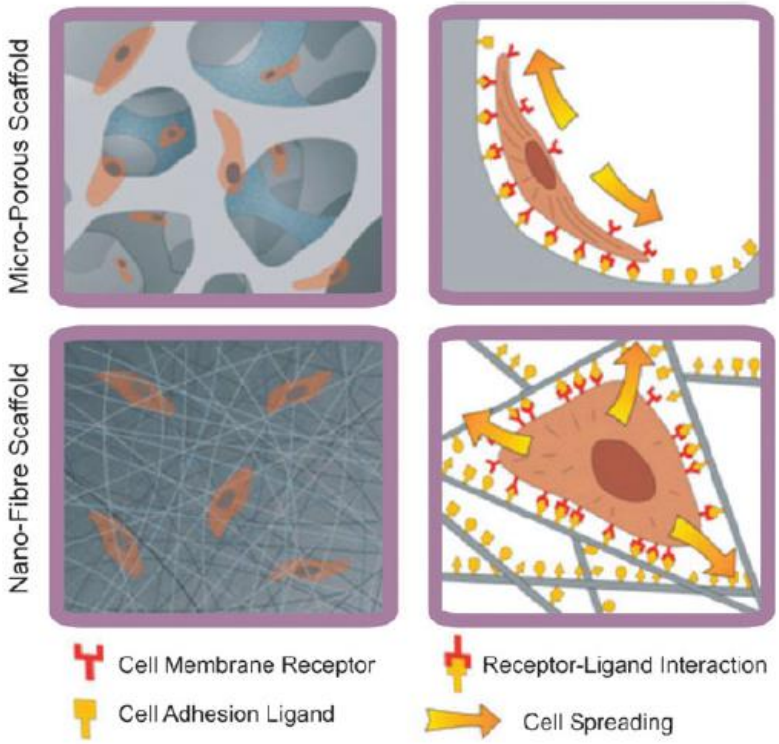

Figure 1.2: Cell-matrix interactions in microporous and nanofibre incorporated scaffold.[30]

1.3 Biomaterials for Tissue Engineering

To accommodate the above mentioned requirements, potential materials for TE scaffolds have been investigated, including natural polymers, synthetic polymers, ceramics, and composite materials.[16] The use of hydrogel networks engineered from polymers are widespread. Hydrogels for cell culture can be formed from a variety of natural and synthetic materials, offering a broad selectivity of mechanical and chemical properties. Hydrogels provide 3D hydrophilic networks of crosslinked macromolecules that can absorb significant amount of water from 10% to thousands of times of their dry weight.[37] This gives them desirable properties such as low interfacial tension with their surroundings and similar properties found in the highly hydrated macromolecular-based materials in human body.[38] As the term “network” suggests, crosslinkers

are needed to prevent hydrophilic materials from dissolving in the aqueous phase. When dry hydrogels are placed in water, water molecules will first interact with hydrophilic and polar groups to form primary bounded water.[39] The network begins to swell and cause the exposed hydrophobic groups to bind with water molecules through secondary interactinos.[39] After the hydrophobic groups fully interact with water, the system will absorb additional water due to an osmotic driving force that maintains a dynamic equilibrium swelling level. As a result, these water molecules are entrapped between chains, pores, and voids. Hydrogels can also be described from a rheological perspective.[39] Below the critical entanglement concentration, hydrogels are in the diluted state, where the average distance between two chains is larger than their sizes. In this state, hydrogels display Newtonian behaviors. Once the concentration reaches the critical entanglement concentration, the polymer chains start to entangle and demonstrate viscoelastic properties. In general, natural hydrogels are biocompatible and can incorporate cells, growth factors, and other bioactive compounds homogeneously. They also allow the diffusion of nutrients and metabolites. Extracellular matrix based hydrogels provide an adhesive surface for cell activity. However, weak mechanical strength and limited degradation rate control are the drawbacks of natural hydrogels.[1] Synthetic hydrogels possess controllable mechanical properties but typically most synthetic hydrogels have weak biocompatibility and biodegradability. Overall, the combination of natural and synthetic hydrogels is appealing options for TE.

1.3.1 Synthetic polymers

Among these materials, synthetic polymers are receiving increased attention even though it has been widely used for tissue engineering. Synthetic polymers can be produced on a large scale while systemically controlling their strength, stiffness, degradation rate, and microstructure properties. The most common biodegradable synthetic polymers are polyesters, polyanhydride, polyorthoester, polycaprolactone, polycarbonate, and polyfumarate.[40] The first requirement of biomaterials is biocompatibility. Hydrophilic polymers, such as poly (ethylene glycol) (PEG) and poly (ethylene oxide) (PEO), with excellent solubility and high solution mobility are ideal for TE. PEG is a Food and Drug Administration (FDA)-approved material and can be conjugated with other functional groups.[6] The degree of crosslinking of PEG-based

materials can be controlled and customized to the desire mechanical properties. Secondly, because one of the main goals of TE is to use a biodegradable non-toxic scaffold as a template for tissue remodeling, the degradability of the scaffold needs to be highly considered. Polyanhydride and polyorthoester degrade by surface erosion, making them suitable for drug delivery. The degradation rate can be controlled by the polymer's glass transition temperature (T_g) and crystallinity because both of the factors influence water penetration. A high T_g and crystallinity can cause limited molecular motion inside the scaffold and lead to low biodegradation rate. The T_g can be tuned by incorporating backbone phenol moieties or bulky side groups in the polymer chains. Similarly, the addition of short side chains or random copolymerization can be used to reduce crystallinity. Polyesters that are degraded by hydrolysis to release oligomers or monomers that can contribute to the metabolic pathways, are widely used in artificial scaffolds. However, these polymers are not best candidates because their hydrophobicity can lead to poor wetting and lack of cell attachment and interaction.[30] Another popular polymer is Pluronic 127, a triblock copolymer with a hydrophobic poly (propylene) (PPO) and two hydrophilic PEO arranged in a PEO-PPO-PEO configuration. This polymer has a thermoreversible gelation behavior when its concentration is over 15 wt%. Pluronic can easily be removed below 4-5 ℃ and form gels over 16 ℃, and thus it can be used as a sacrificial bioink.[6,41–43] However synthetic polymers still lack the biological cues inherent in a variety of natural polymers, such as the lack of active binding sites that can lead to low cell viability.[44] To improve the cell behavior in these polymers, bioactive compounds, like peptide and growth factors, are added or grafted to the network. The peptides provide binding sites for the cells to attach, whereas the growth factors induce cell differentiation to develop into a specific tissue.

Barry et al. reported the fabrication of 3D hydrogels scaffolds through the 3D printing of an acrylamide-based ink. They combined photopolymerization with DIW to produce hydrogel scaffolds in the micrometer size. By suspending 3T3 fibroblasts into the 3D scaffolds, they demonstrated the cells' cytocompatibility and observed the interactions between the adjacent fibroblast cells as shown in Fig 1.3 a and b.[45] Shepherd et al. also fabricated 3D microperiodic scaffolds by using the photopolymerizable hydrogel ink poly (2-hyroxyethyl methacrylate) (pHEMA). The scaffolds offered an ideal environment for

primary rat hippocampal neurons to grow and differentiate through the absorption of polylysine as shown in Fig 1.3c.[46] These researches suggest that synthetic polymer-made scaffolds offer new opportunities for 3D cellular studies. Wu et al. succeeded in fabricating microvascular networks using Pluronic F127. Pluronic F127 was removed by liquefaction at 4 ℃ to yield the desired microchannels within a chemically crosslinked hydrogel matrix (Fig. 1.3d).[42] Kolesky et al. also fabricated vascularized tissue constructs with more advanced engineered scaffolds replete with vasculature, multiple types of cells, and ECM. They used GelMA as the matrix material because of the improved migration and adhesion properties due to the presence of integrin-binding motifs and matrix metalproteinase sensitive groups. Human neonatal dermal fibroblasts (HNDFs) and 10T1/2 were suspended in GelMA while human umbilical vein endothelial cell (HUVEC) was suspended in fugitive Pluronic F127. A construct printed with these bioinks are shown in Fig 1.3 e and f. After 7 days, Kolesky and his coworkers have found the cells in the bioink exhibit similar levels of cell viability as the cells in culture, suggesting that the bioinks and bioprinting approach is non-destructive to the cells.[43]

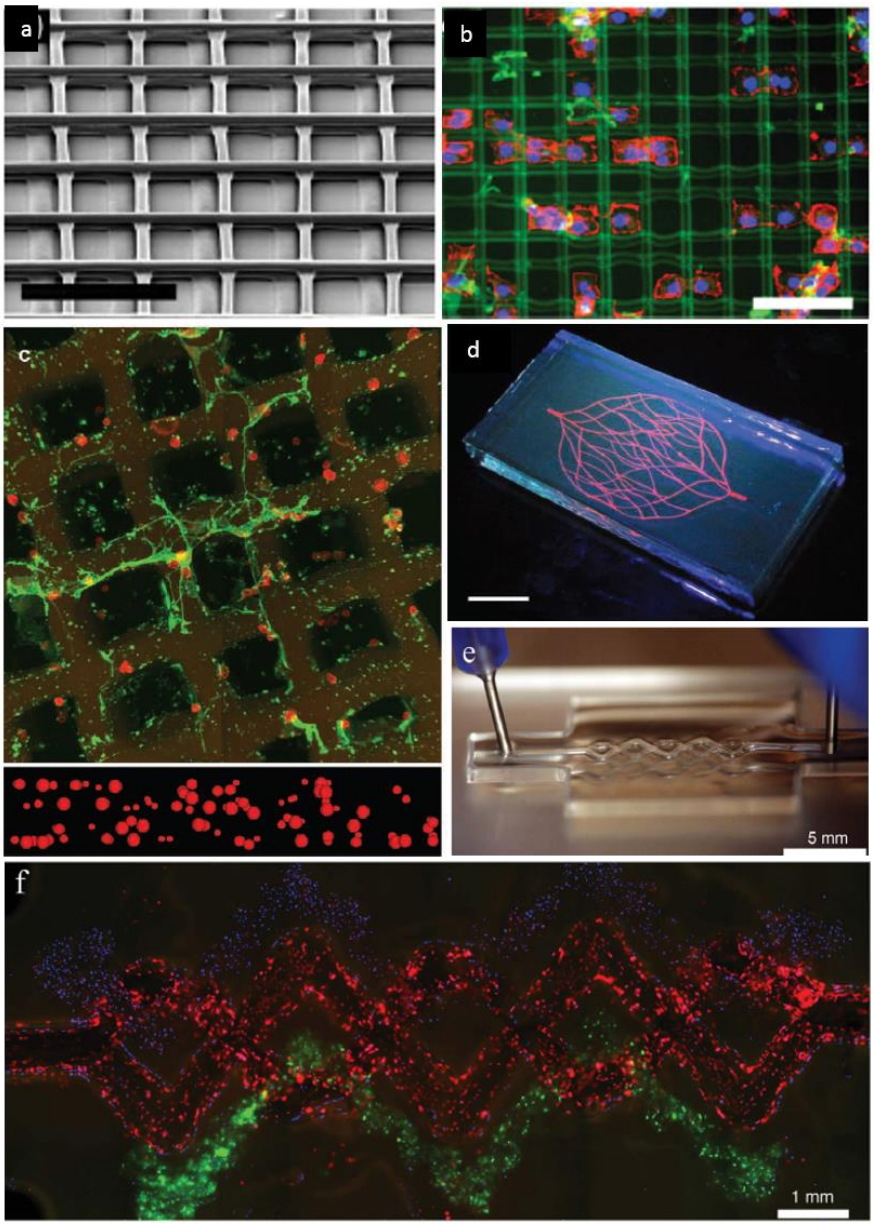

Figure 1.3: (a) SEM image of 3D acrylamide-based ink and pHEMA scaffold. (b) Fluorescence microscopy image of 3T3 fibroblasts suspended in acylamide-based hydrogel scaffold. (c) Confocal images of primary hippocampal cells within the pHEMA scaffold. (d) Fluorescence image of a 3D microvascular network within a hydrogel reservoir (Pluronic F127-diacrylate) and the fugitive ink is liquefied and removed under moderate vacuum. (e) Side view of a microvascular network printed by GelMA and fugitive Pluronic F127 during extraction of fugitive ink. (f) Fluorescence image of the 3D printed tissue construct using three different fluorescent channels: HUVECs (red), HNDFs (green), and 10T1/2 (blue). [42,43,45,46]

1.3.2 Natural polymers

Natural polymers, such as protein-based polymers (collagen, fibrin, gelatin, and synthetic polypeptide)

and carbohydrate-based polymers (alginate, agarose, hyaluronate, chitosan, and dextran),[1] have been used to repair nerve, skin, and bone tissues because they have similar properties to tissues *in vivo*.[47] Natural materials exhibit better cell affinity and structural similarity to native tissues than synthetic materials. However, scaffolds made from natural polymers tend to have poor mechanical strength, which makes them hard to produce.

Collagen is an attractive material for TE and there are at least 19 types of collagen.[48–50] Collagen hydrogels can promote thermoresponsive gelation under physiological conditions since they contain large amounts of glycine, proline, and hydroxyproline residues. The three basic polypeptide chains wrap around one another to form a three-stranded structure through hydrogen and covalent bonds. Collagen strands can also self-aggregate to form stable fibers.[26] Collagen can be readily degraded by metalloproteases, specifically collagenase and serine proteases, to allow controlled degradation of the fiber in the engineered tissue.

Gelatin, produced from collagen through a denaturation process, is widely used as a gelling agent in food, cosmetics, and pharmaceuticals. It is in the liquid form above 40 ℃ and reversibly forms an α helix structure below 30 ℃ by coiling its molecular structures.[51–53] Gelatin provides an ECM-like microenvironment for cells to embed in as it forms intermolecular triple helices. GelMA can be modified with methacrylate (MA) groups, which will crosslink when exposed to UV light. By changing the degree of modification. GelMA's properties such as viscosity and mechanical strength also varies.[35,47,54]

Fibrin hydrogels have been used widely in tissue engineering, such as liver, cartilage, bone, muscle, skin, and vascular tissues.[55,56] It is a biopolymer composed of monomer fibrinogen. Two sets of three polypeptide chains, Aα, Bβ, and γ, are joined by six disulfide bridges to form the fibrinogen molecule. The fibrin is formed from the thrombin-mediated cleavage of fibrinopeptide A from the Aα chains and B from the Bβ chains.[55] Fibrin can turn into gel through the enzymatic interaction between fibrinogen and thrombin, which is also a mechanism for blood coagulation.[57] It can also be modified with active peptides to further mimic the natural matrix. The mechanical and shrinkage properties of fibrin vary depending on the different components and concentrations. However, the poor mechanical strength and shrinkage are the major

disadvantages of fibrin, which can be solved by crosslinking or combining fibrin with other biomaterials.[55]

Hyaluronic acid (HA) is the simplest glycosaminolglycan (GAG) and found in almost every mammalian tissue and fluid. It is a linear polysaccharide composed of a repeating disaccharide of (1-3) and (1-4)-linked β-D-glucuronic acid and N-acetyl-β-D-gulcosamine units.[26] HA can be crosslinked with hydrazide derivatives. Since HA is normally found in the human body, it can be naturally degraded by hyaluronidase. Rodell et al. have studied the effect of supramolecular assembly on the HA properties by the stabilization of the hydrogels and introduction of the second covalent crosslinking. The first reaction occurred between the guest-host pair of cyclodextrin modified HA and adamantane modified HA. With the addition Michael-acceptors, the thiol-modified HA crosslinked covalently to increase the modulus of the hydrogel. They found that the dual-crosslinking HA improved yields, suggesting its potential use in TE.[58]

Chitosan is a linear polysaccharide made up of (1-4)-linked D-glucosamine and N-acetyl-D-gulcosamine residues derived from chitin. Chitosan is structurally similar to GAGs and is degraded by enzyme in humans. Chitosan is soluble in dilute acids and turns into gel by increasing the pH. Chitosan is degraded by lysozyme and the degradation rate is inversely related to the crystallinity determined by the degree of N-deacetylation.[26]

1.3.3 Ceramics

Ceramics are commonly used in biomedical applications due to their high stiffness and bioactivity, which are similar to the mineral phase of native bones. Therefore, they provide a natural and osteoinductive surface for bone tissue development.[59,60] Calcium phosphate ceramics (CPCs) are a class of tunable bioactive materials used for bone tissue repair and augmentation. The most common four CPCs used for bone tissue engineering are hydroxyapatite (HAP), tricalcium phosphate (TCP), amorphous calcium phosphates (ACPs), and biphasic calcium phosphates (BCPs). Michan et al. used concentrated HAP colloidal inks to create 3D periodic scaffolds through the DIW process. [61,62] HAP is the most stable and least soluble material with a solubility product constant of 9×10^{-58} over a pH range of 3.5 to 9.7. Although it is not highly soluble, the surface of HAP can provide nucleating sites that can increase their solubility.[59] Stable ammonium polyacrylate-coated HAP suspensions were gelled with the addition of the poly

(ethylenimine) (PEI) gelling agent. The elasticity of the scaffolds increased with the addition of PEI, which allows the ink-based filaments able to extend the gaps in each layer without significant deformation. By tuning the composition and viscoelasticity of the ink, the HAP scaffolds can be fabricated without sacrificing support materials.[61]

1.3.4 Composite inks

Hydrogels formed from natural materials promote cell functions whereas hydrogels formed from synthetic materials hinder cell functions.[31] Researches showed that synthetic gels can function as 3D cell culture scaffolds. However, they lack active integrins, surface receptors and endogenous factors that promote cell activities. Natural hydrogels are typically derived from natural sources and are consisted of proteins and ECM components, so these gels are inherently biocompatible and bioactive. Endogenous factors promote cellular functions and are vital for the cell viability and development of many cell types. However, because natural scaffolds are complex, it is hard to determine which factor promotes cellular function. Moreover, it is difficult to tune the mechanical and biochemical properties of the natural hydrogels. (Fig. 1.4) By virtue of these obstacle, natural and synthetic polymers are combined together to produce a desirable materials for TE. In addition, the electrical conductivity of these scaffolds at biologically relevant frequencies is too low to transmit signals. Moreover, the polymeric scaffold often lacks the 10-100 nm nanofibrous structures usually found in abundance in native ECM that can regulate cell behavior. To address the shortcomings of polymeric scaffolds, nanomaterials are being explored and incorporated in the TE scaffolds to improve cell adhesion, cell viability and 3D cellular self-assembly, so a new design of composite inks also emerged.[35] The goal of the composite inks is to enhance the ink properties, such as mechanics, printability, and bioactivity.

Synthetic and natural polymers are combined together to make an optimized pre-gel solution. Armstrong et al. have demonstrated the feasibility of 3D printing of Pluronic-alginate multicomponent bioinks.[63] With the addition of Pluronic F127 in alginate, the hybrid bioink showed improved shear thinning behavior, compressive modulus, and shear modulus, which provides a platform for bioextrusion. No significant loss in the viability of the encapsulated human mesenchymal stem cells (hMSCs) was observed

over a 10-days period. The incorporation of Pluronic F127 into alginate matrices also increased the porous architecture because the fugitive Pluronic F127 were then removed after the engineered scaffolds formed. This indicates that the fugitive ink did not only provide a microscopic structure formation, but also template a macroscopic structure. Their research illustrated the possibility of printing tissue constructs with complex physiological structures.

Graphene-derivatives and CNTs offer the advantages of improved mechanical properties and electrical conductivity while maintaining biocompatibility of the hybrid biomaterials. Works have been done on graphene-derivatives and CNTs to demonstrate their applications in tissue engineering. Shin et al. have demonstrated the enhancement of cellular performance, mechanical properties, and electrical properties after the incorporation of CNTs and graphene-derivatives into photo-curable GelMA hydrogels.[35,47,54,64] It was found that the incorporation of CNTs into the hybrid matrix increased the compression modulus from 10 kPa, without CNTs, to a maximum of 32 kPa with 3 mg/mL of CNTs. They also demonstrated that the CNTs did not change the porosity of the polymeric matrices but increased the size of the pores as the concentration increases.[35,47] Cha et al. found that the cell viability remained high and cells were able to spread and proliferate throughout the experimental period. Furthermore, the incorporation of graphene oxide (GO) in GelMA matrices caused higher proliferation rate due to the graphene-based materials.[54]

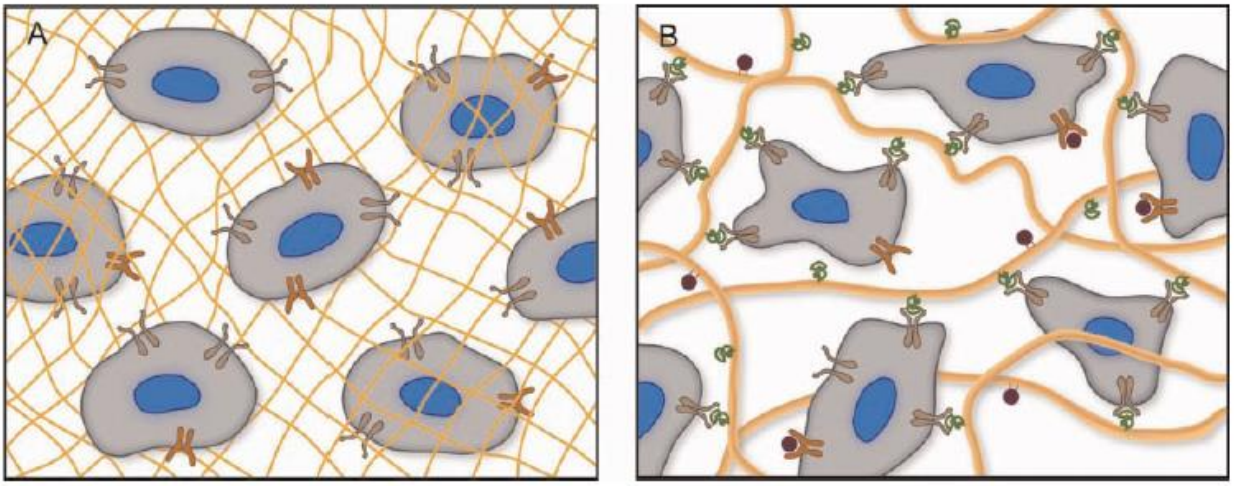

Figure 1.4: (A) Scaffold formed of synthetic polymers (yellow mesh) provide a 3D environment for culturing cells, but they fail to activate integrins (brown) and other surface receptors (orange). (B) Scaffold formed of naturally derived polymers contains a large amount of integrin-binding sites (green) and growth factors (red) coordinated to the ECM (yellow fibers).[31]

1.4 Requirements of Hydrogels for Bioextrusion Printing

Although 3D printing offers great potential for TE, there are still some issues to overcome. One of the challenges is the capabilities of the 3D printers. Extrusion rate, printing speed, and printer resolution are keys for the optimal level of artificial tissue constructs. Another major issue is the suitability of the printable bioinks. Overall, the biomaterials suitable for bioextrusion are required to flow easily under pressure, gel quickly or retain their shape for a long time, and maintain sufficient integrity after fabrication. However, the characteristics of the scaffolds may not work well with each other. For example, soft materials can be extruded through a nozzle and degrade easily, but this can cause difficulties in handling. In bone tissues, stiff materials are used for osteoblast development and bearing loading, however, its printability and degradability are of concern. A balance between all of the parameters should be achieved to create the appropriate printable biomaterials.

The major parameters that determine the printability of a hydrogel are rheological properties and crosslinking mechanism.[44] Meanwhile, other specific parameters, such as nozzle gauge and pressure on the piston, will determine the shear stress on the encapsulated cells and the time required for the fabrication of a designed scaffold (Fig. 1.5). Finally, after the pre-gel solution are extruded, the printed constructs should have the proper mechanical strength and shape fidelity for processing. For bioextrusion, the constructs printed by high viscous inks will retain their initial shapes for the subsequent gelation process.

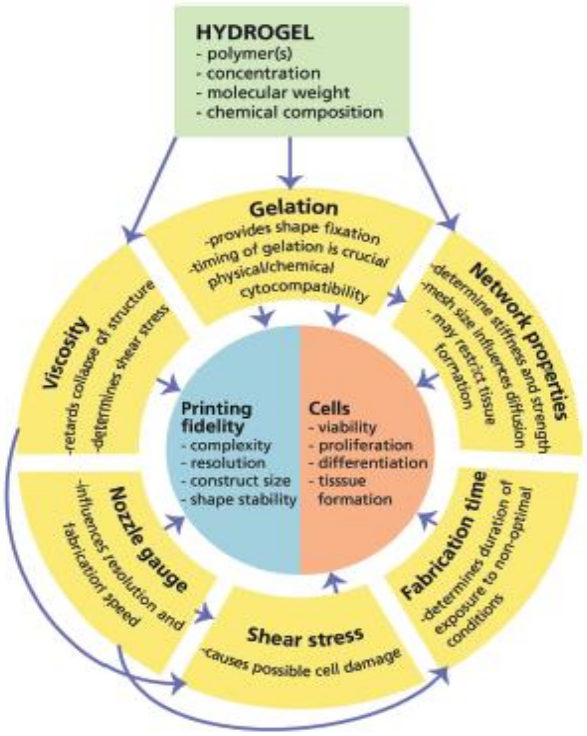

Figure 1.5: Concept map of variables and relations critical to biofabrication. The hydrogel (polymer type(s), concentration, molecular weight and chemical composition) directly determines the viscosity, gelation mechanism and speed, and mechanical properties of the final gel. This -in combination with processing parameters, such as nozzle gauge and fabrication time- influence the main outcomes Printing fidelity and Cell viability and function.[44]

1.4.1 Viscosity

The viscosity of a polymer pre-gel solution is predominantly determined by the polymer concentration and molecular weight. Hydrogels of high concentration will restrict various cell behaviors, such as cell migration, proliferation, and differentiation. Thus lowering the high molecular weight polymer concentration is desirable. Generally, viscosity influences the scaffold's fidelity after deposition by increasing the shape's fidelity as the viscosity increases. However, high viscosity means that there is high shear stress on the encapsulated cells, which is harmful to the cells. Viscoelastic hydrogels are required for bioextrusion and thus injectable, shear-thinning hydrogels are a subgroup of hydrogels but form the majority of those used in bioextrusion.[65,66] These kinds of hydrogels have proper viscosity to flow through a pressurized nozzle without clogging and span gaps in each layer. Strong shear-thinning liquids are good candidates for bioextrusion because they have high viscosities at low shear rates, which allows hydrogels

to form intricate patterns when extruded and while at high shear rates, they possess low viscosities and can easily flow through the nozzle.[45,67–69]

The viscosity of Newtonian materials does not depend on shear rate unlike non-Newtonian liquids. In the vast majority of cases, viscosity decreases as the shear rate increases within a certain range in a phenomenon called shear-thinning behavior. It is caused by shear-induced reorganization of the polymer chains to a more stretched form. The viscosity-versus-shear rate curves of this kind of materials show that at very low shear rates the viscosity is constant, while at high shear rates region, the viscosity is constant at a lower level. In the shear-thinning region, the relationship between shear rate and viscosity is shown below:

$$\eta = K\dot{\gamma}^{n-1}. \tag{1.1}$$

This is the well-known *"power-law"* model and n is termed as the power-law index. K is called the consistency. η is the viscosity, and $\dot{\gamma}$ is the shear rate. The equation shows that the slope of the shear-thinning region is equal to $n-1$ if the x-axis and y-axis are in the logarithmic form.[70]

In addition, the hydrogel inks are designed to crosslink immediately after printing or retain their shape for a long time, which is related to the complex shear modulus G^*, elastic modulus G' and viscous modulus G''.[70] These parameters can be obtained through an oscillatory test. G^* is defined through the following equation:

$$\sigma(t) = G^*\gamma(t), \tag{1.2}$$

where σ and γ are the shear stress and shear strain varied with time, respectively. The G' and G'' are obtained from G^* through the following equation:

$$G^* = G' + iG''. \tag{1.3}$$

G' and G'' are also called the elastic and viscous modulus, respectively. If $G' < G''$, the material possess the liquid behavior.

If a non-Newtonian liquid flows through a straight circular tube of a radius r at a volume flow rate Q, the shear rate at the wall is modified to:

$$\gamma_w = \frac{4Q}{\pi r^3}\left(\frac{3}{4} + \frac{1}{4}\frac{d\ ln\ Q}{d\ ln\ \sigma_w}\right). \tag{1.4}$$

When a shear-thinning liquid is tested, $\frac{d\ ln\ Q}{d\ ln\ \sigma_w}$ is greater than 1 and the power-law liquid is equal to $1/n$.[46] So the shear rate at the wall can be written briefly as:

$$\gamma_w = \frac{4Q}{\pi r^3}\left(\frac{3}{4} + \frac{1}{4n}\right). \quad (1.5)$$

1.4.2 Crosslinking mechanisms for hydrogels

Gelation of the printed constructs is necessary for the constructs to retain their shapes. The hydrogels could be crosslinked physically or chemically upon external stimulus, such as light, temperature, or ion concentration.

Physical crosslinking mechanisms rely on non-chemical interactions, such as ionic interactions, hydrogen bonds, hydrophobic interactions, and thermal response. For example, alginate is an ionically crosslinked polymers, that is highly soluble in water as Na-salt. Upon the addition of Ca^{2+}, alginate gels rapidly. Physically crosslinked hydrogels are not stable since the reactions are reversible and can be disrupted by changes in pH, temperature, and ion concentrations. However, physically crosslinked hydrogels are the dominant biomaterials used for bioextrusion. One reason is because the absence of extra chemical agents from the crosslink process of physically crosslinked hydrogels decreases the material toxicity. In recent years, the electrostatics interactions between opposite charged particles in hydrogels have been exploited. Rapid gelation occurs upon mixing but liquefies over a certain shear stress, at which the interactions between oppositely charged particles are broken.[5,44]

Chemical crosslinking mechanisms depend on newly formed covalent bonds. The covalent bonds are usually formed by mixing two reagents, such as monomers and initiator, and two reactive chemicals (e.g., Mannich reaction). Chemically crosslinked hydrogels are stable for a longer term when compared to physically crosslinked hydrogels. In addition, the mechanical strength of the chemically crosslinked hydrogels can be controlled by the crosslinking density. The most common method used for the bioextrustion of pre-gel solution is photopolymerization. However, the cell viability will decrease due to the exposure to UV light and free radicals. In addition, the pre-gel solution can clog the nozzle during printing if it is exposed to light.

Considering the advantages and disadvantages of physically and chemically crosslinked methods, attention should be focused on hydrogels that can interact through weak physical interactions and then further crosslinked through chemical interactions. The purpose of the first physical crosslink process is to tune the viscoelastic properties and primary shape retention. The chemical interactions help post-processing fixation and stabilization of printed constructs. In this type of systems, gelation mechanisms are often involved.[44] For example, warm GelMA-based solutions initially gelate due to cool temperatures and then crosslinked by UV-curing. As mentioned before, this type of method has potential side effects on the embedded cells; therefore other methods to crosslink hydrogels, such as the infrared-induced polymerization, need to be discovered.

Chapter 2: Hydrogels Incorporating Cellulose Nanocrystals for Mechanical Reinforcement

2.1 Introduction

This chapter includes the work done on the mechanism of crosslinking of alginate and the effect of functional nanomaterials on the mechanical properties of the hydrogel. The incorporation of cellulose nanocrystals into pure alginate systems through physical interaction was investigated. In addition, the modification of alginate was performed to produce a more stable system.

2.1.1 Alginate

Alginate is a natural linear polysaccharide from seaweed composed of (1,4) β-D-mannuronic (M) and α-L-guluronic (G) acid residues.[71–75] The block copolymers consist of M-blocks, G-blocks and MG-blocks. The amount and sequence of the blocks determine the chemical and physical properties of alginate. In aqueous solution, G-blocks of different alginate chains are able to form a cooperative "egg-box structure" by trapping divalent cations (e.g., Ca^{2+}, Sr^{2+}, Ba^{2+}),[71] where two polymer chains are linked to form alginate hydrogels. On the other hand, monovalent cations (e.g., Na^{+} and K^{+}) or magnesium cannot act as crosslinkers.[71] The inflexibility of different blocks in alginate molecules increases such that GG<MM<MG. Furthermore, its viscosity depends on the molecular weight.[73]

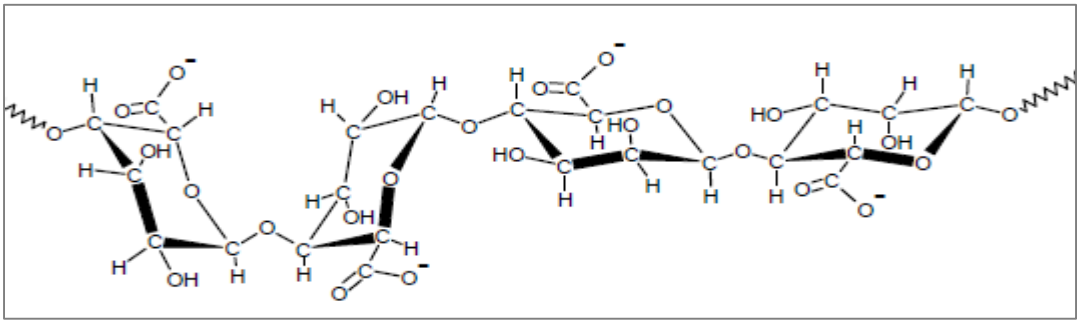

Figure 2.1: Chemical structure of alginate.

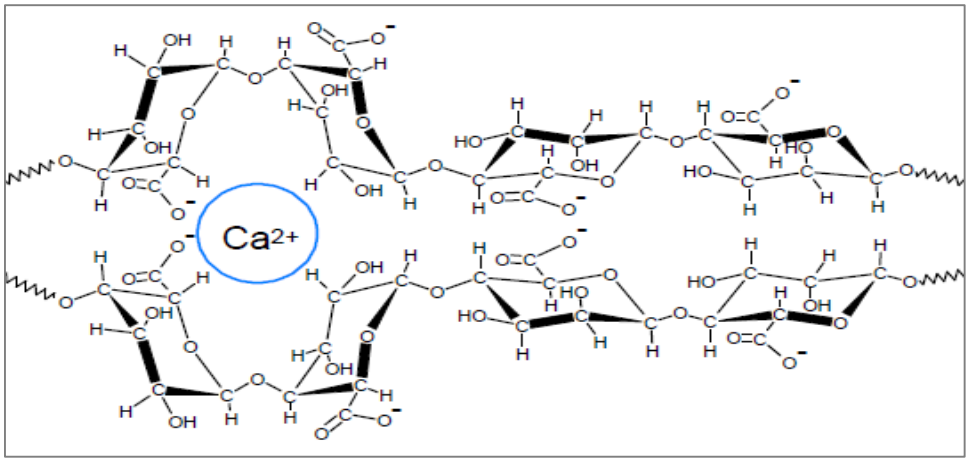

Figure 2.2: Schematic representation of the egg-box structure of the alginate crosslinked by calcium ions.

In general, physically crosslinked alginate hydrogels lose more than 60% of their initial mechanical strength within 15 hours of exposure to physiological buffer due to the exchange of divalent and monovalent ions from the surrounding environments.[38,74] There is also limited control over the mechanical properties, swelling ratios and degradation rates for the ionic crosslinked alginate hydrogels.[76]

To resolve the aforementioned issues with the physically crosslinked alginate hydrogels, photocrosslinked hydrogels are gaining increased attention in tissue studies. With the controlled exposure time and the proper photoinitiators, the damage to cells and bioactive molecules can be greatly minimized.

Alginate has an abundance of available hydroxyl (-OH) and carboxyl (-COOH) groups along its backbone, making it possible for various chemicals to functionalize for better solubility, hydrophobicity, and physicochemical and biological properties. Much research has been done on the modification of alginate, including oxidation, reductive-amination of oxidized alginate, sulfation, copolymerization, esterification, and amidation.[77] Among these methods, Jeon's group found that 2-aminoethyl methacrylate (AEMA) is a good crosslinker due to its biodegradable ester groups. The swelling ratios and degradation rates can also be controlled by changing the degree of alginate methacrylation.[76]

2.1.2 Cellulose Nanocrystals

Cellulose, the most abundant substance on earth, is considered as an inexhaustible source of raw materials.[78,79] It is a linear syndiotactic homopolymer composed of β-(1, 4)-glycosidic bonds linked D-

anhydroglucopyranose.[78–86] Cellulose is a straight chain polymer, unlike some polysaccharides that can coil and branch out. Cellulose fibers exist in a variety of organisms such as wood, plants, tunicates, algae, and bacteria. Cellulose chains are connected to each other via hydrogen bond and van der Waals force, to form elementary fibrils that are further assembled into microfibrils of 5-50 nm in diameter and several micrometers in length. These microfibrils consist of highly crystalline regions alternating with amorphous regions. When cellulose fibers are subjected to certain mechanical and chemical treatments, the highly ordered regions can be extracted, resulting in the cellulose nanocrystals (CNC).[78,87] The two most common methods to isolate CNC are mechanical process and chemical hydrolysis. Mechanical process includes the use of high-pressure homogenizers, grinders/refiners, cryocrushing, high-intensity ultrasonic treatments, and microfluidization. The most popular and common chemical hydrolysis is acid hydrolysis. Acid is typically used to hydrolyze and disrupt the disordered or paracrystalline regions while the crystalline regions with a higher resistance to acid treatment remain intact. After allowing the reaction to occur for a certain amount of time, the mixture is diluted with water, centrifuged, and washed for several times, followed by dialysis against deionized water to remove unreacted chemicals. An additional centrifuge step is used to remove any larger agglomerates. Sulfuric and hydrochloric acids are the most common acids used in acid hydrolysis. CNC extracted by different acids show significant differences in the dispersity and stability. For example, CNC derived from sulfuric acid hydrolysis show higher solubility in water due to the negatively-charged sulfate ester surface.[87]

CNC are rod-like or whisker-shaped nanoparticles with an average diameter of 5-10 nm and an average length of around 100 nm.[78,88] CNC possess some promising properties such as renewability, low density, high mechanical strength, large and highly reactive surface (250~500 m^2/g), and low cytotoxic response. The van der Waals force and intermolecular hydrogen bonds promote the stacking of cellulose chains that cause the CNC's crystalline structure. Due to the high crystallinity, CNC exhibit an axial elastic modulus ranging from 110 to 220 GPa and a tensile strength ranging from 7.5 to 7.7 GPa.[78] Thus, CNC can be used to mix into various polymer matrices to reinforce the mechanical strength of gels. The rheological property of cellulose nanocrystals is another promising property for 3D bioprinting. In diluted CNC solution,

shear thinning behavior is observed due to the alignment of the chiral nematic liquid crystalline domains.[87,89]

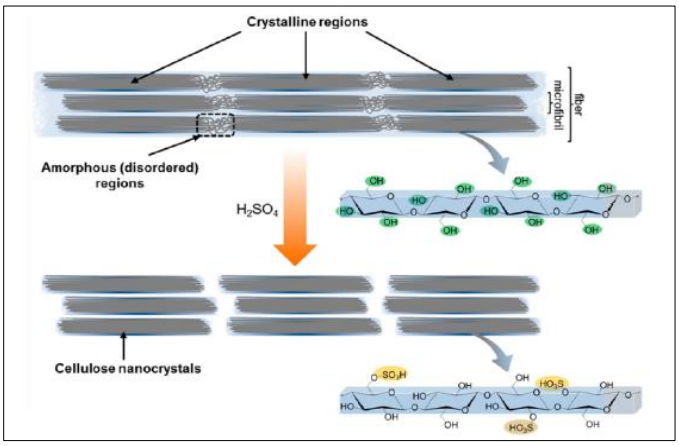

Figure 2.3: Schematic showing cellulose fibers containing alternate crystalline and amorphous regions and negatively-charged CNC after removing the amorphous regions of cellulose fibers through acid hydrolysis.[78]

The abundance of hydroxyl groups on the backbone of cellulose nanocrystals allows the possibility of its modification. All the chemical modifications can be divided to two parts: (1) introduce stable opposite charge on the surface of CNC to obtain better dispersion; (2) modify the surface to improve their compatibility.[80,87] After modifying the surface, the physical and chemical properties of the cellulose can be changed. Noncovalent surface modification is typically achieved through the adsorption of surfactants to increase the dispersibility of CNC in organic media. The interactions between the modifiers and cellulose nanocrystals include electrostatic attraction, hydrogen bond, or Van der Waals forces. The surface covalent modifications include carboxylation, esterification, silylation, sulfonation, oxidation, cationizaiton, and polymer grafting. Since cellulose nanocrystals are insulators, the synthesis of conductive CNC is highly desired to form conductive tissue scaffolds. π-conjugated polymers have been found to be electrically conductive for decades. Such intrinsically conductive polymers (ICPs) including PPy[90], PANI[91], poly(3,4-ethylene-diocythiophene)[92], and poly (p-phenylene ethylene) (PPE)[93] are good candidates for the formation of conductive CNC.

Some recent works have demonstrated the application of CNC in tissue engineering, such as drug delivery, antimicrobial and medical applications, and biosensors and bioimaging.[82,85] The incorporation of CNC in the scaffold matrix is to enhance mechanical properties, electrical conductivity, and introduce

adhesive moieties to enable cell activities. Dugan et al. have demonstrated the potential use of CNC in tissue engineering.[94] It was shown that CNC promotes the growth of myoblasts and enhances the degree of myoblast fusion. These results highlight the use of CNC in tissue engineering for guiding cell behavior.

2.2 Materials and Methods

2.2.1 Materials

Pharm grade sodium alginate (PROTANAL LF 10/60 FT) with the amount of G residue of 60-70% was a product sample from FMC. Cellulose nanocrystals hydrolyzed from wood were donated from Professor Michael Tam's group. 2-aminoethyl methacrylate (AEMA), 2-morpholinoethanesulfonic acid (MES), sodium hydroxide, sodium chloride, calcium chloride, acetone and deuterium oxide (D_2O) were purchased from Sigma-Aldrich. N-hydroxylsuccinimide (NHS) and 1-ethyl-3-(3-dimethylaminopropyl)-carbodiimide hydrochloride (EDC) were purchased from Alfa Aesar and G-biosciences, separately.

2.2.2 Fabrication and characterization of alginate-CNC (ALG-CNC) hydrogels

CNC were well dispersed in an alginate solution to form a hybrid hydrogel solution. Samples of different concentrations of alginate ranging from 1% (w/v) to 4% (w/v) were prepared. Various concentrations of CNC solution, up to 1% (w/v), were added to 1% (w/v) alginate solution and mixed by a dispenser for 5 min. A custom-made teflon mold was filled with the polymer solutions and then immersed in a $CaCl_2$ bath to form consistently-sized samples. These hydrogels were then stored in $CaCl_2$ solution for mechanical tests.

Unconfined compression testing was performed on a TA XT Plus Texture Analyser (Stable Micro Systems). Air bubbles were first removed and the prepared samples were examined for physical defects. The dimensions of each samples were measured with calipers. The compression speed and compressibility was set as 0.05 mm/s and 90%, respectively. The compression modulus was obtained from the slope of the first 10 % of the stress-strain curves.

2.2.3 Synthesis and characterization of methacrylated alginate (MAALG)

MAALG was prepared by mixing the alginate solution with 2-aminoethyl methacrylate (AEMA).

0.05 M MES (60 mL) containing 0.5M NaCl was prepared followed by the addition of 500 mg alginate. After the alginate was well dissolved, NHS (132.5 mg) and EDC (437.5 mg) were added into the flask. After 5 min, AEMA was mixed with alginate at the molar ratio of NHS: AEMA=1:1. The pH of the mixture was carefully adjusted to 7.5 with NaOH solution. The reaction was carried out at room temperature overnight. The mixture was precipitated with the addition of an excess amount of acetone, dried under reduced pressure and rehydrated to a 1% (w/v) solution in Milli-Q water. The MAALG was purified by dialysis against Milli-Q water for a week and then lyophilized.

The synthesized MAALG was dissolved in D_2O and placed in a nuclear magnetic resonance (NMR) tube. The ^1H NMR spectra of alginate and MAALG were tested on a 300 Hz NMR (Bruker, Advance III).

2.3 Results and Discussion

2.3.1 Mechanical properties of ALG-CNC hydrogels

The concentration of nanoparticles as reinforcing materials within the polymer matrix is critical for enhancing the mechanical strength of the polymer composites. The hydrogel solutions became whiter with increasing amount of CNC. The mechanical properties of the pure alginate hydrogels and the hybrid hydrogels were evaluated by uniaxial compression test. The load to impose a given compressibility is monitored as the specimen is compressed at a constant rate, generating a load-versus-compressibility profile.

The resulting stress-versus-strain curve is given where the stress, σ, is defined as

$$\sigma = \frac{P}{A_0}, \tag{2.1}$$

where P is the load on the sample with an original cross-sectional area A_0. The strain, ε, is defined as

$$\varepsilon = \frac{l - l_0}{l_0}, \tag{2.2}$$

where l is the gage length at a given load, and l_0 is the original length.

Elastic modulus, E, is determined by the slope of the stress-strain curve in the elastic region. The linearity of the stress-strain plot in the elastic region is a graphical statement of Hooke's law:

$$\sigma = E\varepsilon. \tag{2.3}$$

Herein the modulus, E, represents the stiffness of a material.[95]

The mechanical strength of these hydrogels was evaluated by a uniaxial compression tester (Fig. 2.4). Samples were placed in the center of the stage to ensure a stable force received.

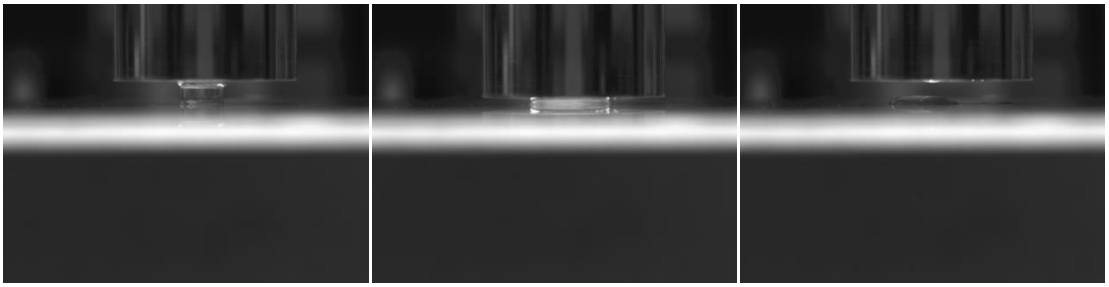

Figure 2.4: CNC-incorporated alginate hydrogel subjected to uniaxial compression in the beginning, in the middle, and after the compression (from left to right).

The area below the curve corresponds to the toughness of the materials. Fig. 2.5A implies that the toughness of alginate hydrogels increased with the increasing concentration of the alginate. By taking the initial 10% of the stress-strain curve, the compression modulus was acquired. The elastic modulus of alginate (Fig. 2.5B) increased from 79 kPa to 470 kPa, as the concentration of alginate increased from 1% (w/v) to 4% (w/v).

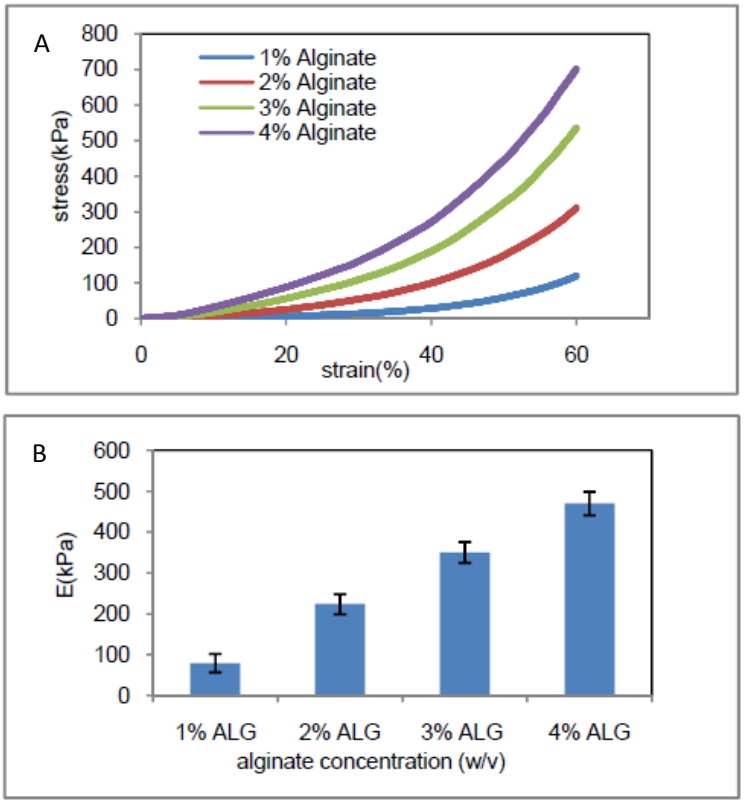

Figure 2.5: (A) Stress-strain curves of alginate hydrogels of different concentrations measured with a uniaxial compression tester. (B) Elastic modulus of alginate hydrogels.

The presence of CNC had a profound effect on the toughness and stiffness of alginate hydrogels and CNC acted as an enhancement agent in the alginate-based hydrogels due to their good affinity with the alginate as shown in Fig. 2.6. With 0.4% (w/v) CNC, the elastic modulus of the hydrogels increased to the maximum of the seven different formulations of 110 kPa from 79 kPa without CNC. However, the incorporation of 1% (w/v) CNC contents raised the elastic modulus of the hybrid hydrogels by only 20%. At low concentrations, CNC could be well dispersed in the alginate, while at high concentrations, the hydrogel showed a lower elastic modulus. The result can be explained by the aggregation of CNC at high concentrations that decreases the mechanical strength.

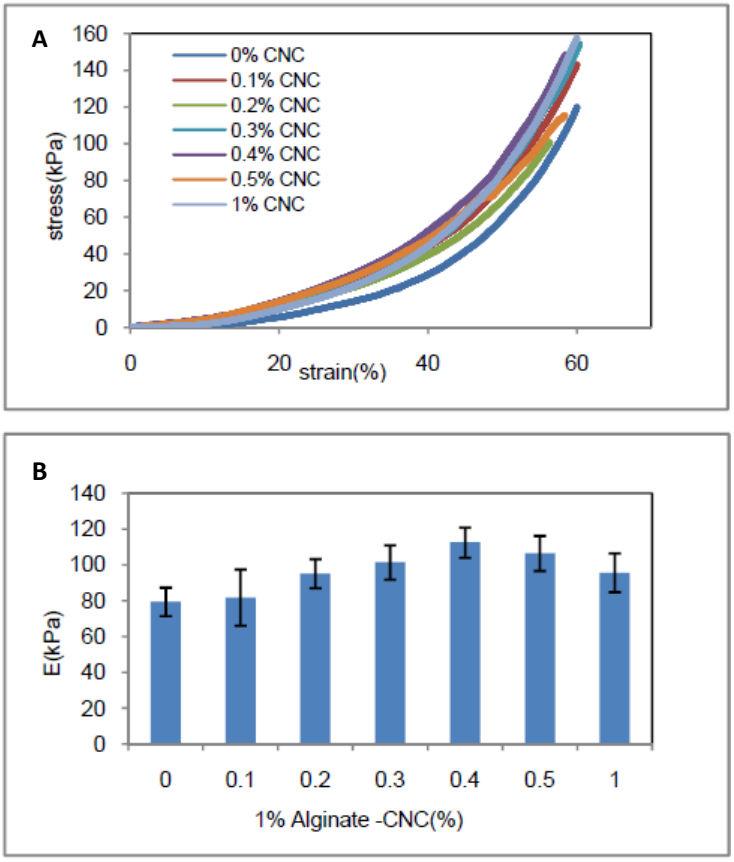

Figure 2.6: (A) Stress-strain curves of 1% alginate hydrogels incorporated with different amounts of CNC measured from uniaxial compression. (B) Elastic modulus of alginate-CNC hydrogels.

2.3.2 MAALG characterization

The ^{1}H NMR spectrum of MAALG is shown in Figure 2.7B. The peaks at δ2.9 and 1.1 ppm are attributed to the residual EDC-urea. The ^{1}H NMR spectrum of MAALG exhibits peaks at δ6.2 and 5.7 ppm, which are due to methyl protons (Figure 2.7B: c). In addition, the peak at δ1.9 ppm represents vinyl methylene (Figure 2.7B: d).

The actual efficiency of alginate methacrylation was calculated from the ratio of the integrals for the vinyl methylene protons (Figure 2.7A: c) to alkyl (C-H) protons (Figure 2.7B: a). In this experiment, it showed that the methacrylation of alginate was 45%.

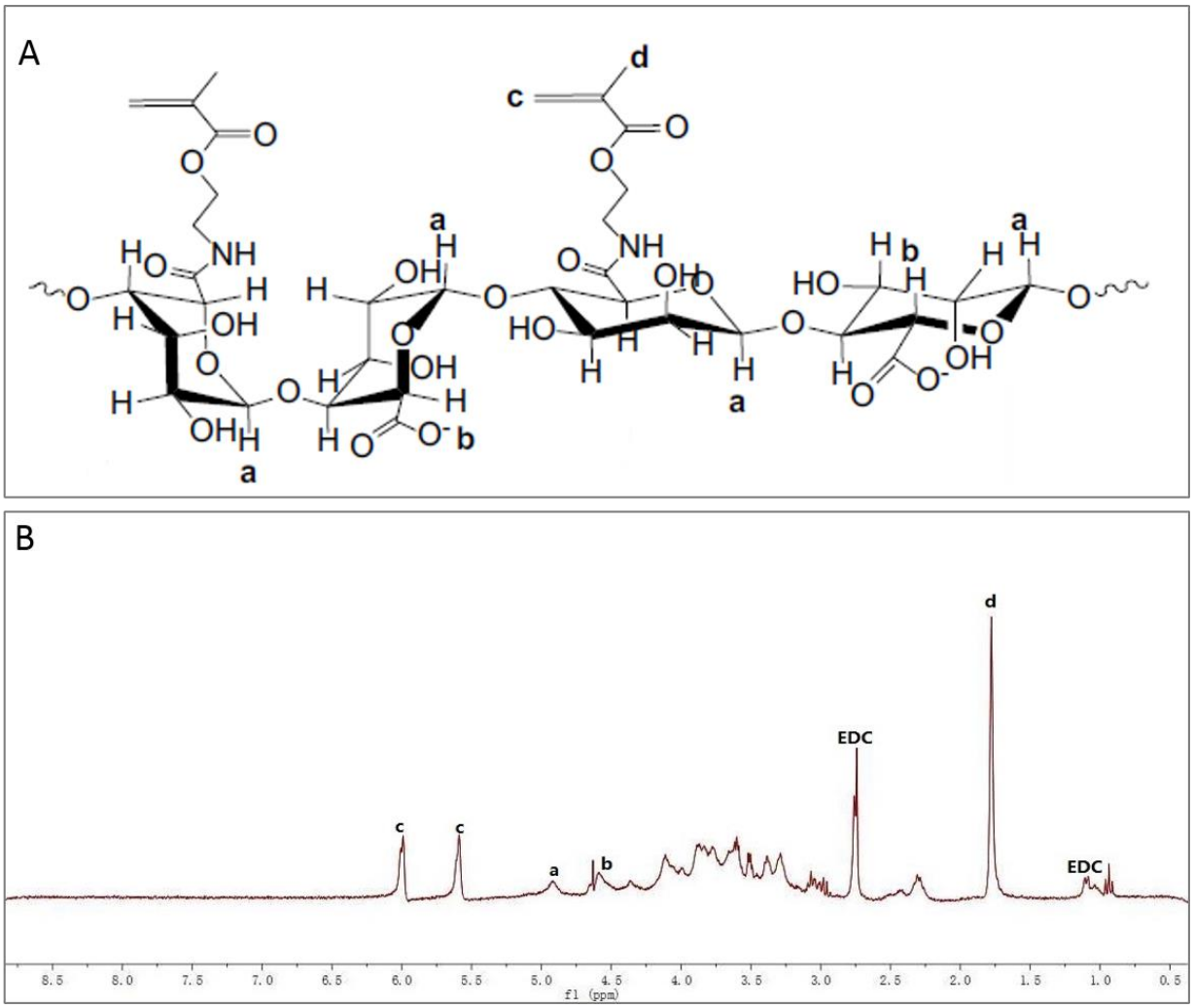

Figure 2.7: (A) Structure of MAALG; 1H NMR spectra of (B) MAALG.

2.4 Conclusions

The work in this chapter was focused on exploring the effect of the incorporation of CNC into a polymer system. It was found that the incorporation of CNC greatly enhanced the mechanical strength of ALG-CNC composite matrix. However, too high concentrations of CNC could also cause reduced mechanical strength, but still higher than pure alginate. The modification of alginate was attempted. Photocrosslinkable alginate was prepared by reacting sodium alginate with AEMA in the presence of NHS and EDC. Current date shows that the reaction was successful. The degree of methacrylation was detected by NMR and the characterization showed that the efficiency could reach about 45%, depending on the ratio of carboxyl in alginate to amine groups in AEMA.

Chapter 3: Hydrogels Incorporating Cellulose Nanocrystals for 3D Printing

3.1 Introduction

In this chapter, a hybrid pre-gel solution was prepared by adding CNC to alginate prior to the characterization of the hybrid solution. The incorporation of CNC into alginate did not only enhance the mechanical properties, but also introduced shear thinning properties that allows the hybrid pre-gel solution to print. The hybrid bioinks were then used for 3D bioprinting and cells were encapsulated in the bioinks to study the behavior of cells. It was deduced that the bioprinting process did not influence the cell viability and that the hybrid bioink is suitable for tissue engineering.

The following section briefly introduces relevant background on the 3D printing of soft hydrogels for tissue engineering. Tissue engineering (TE) scaffolds are required to closely mimic the natural cell environment to enable the study of cell behavior *in vitro* and allow the fabrication of artificial tissue constructs. The structural features of the scaffolds critically influence the differentiation, proliferation rates, migration, and gene expression of cells. 3D bioprinting is a potential approach to create optimal 3D scaffolds using biomaterials. Essential to this approach is the formulation of bioinks that possess the required rheological properties and are also biocompartible. Ideally, the bioinks should show shear thinning behavior by having a high viscosity at low shear rates and a low viscosity at high shear rates. In this research, a hybrid hydrogel solution was created by mixing alginate and cellulose nanocrystal. Alginate, a natural linear polysaccharide isolated from seaweed, is composed of (1,4)β-D-mannuronic (M) and α-L-guluronic (G) acid residues and can crosslink by forming a cooperative “egg-box structure” between G-blocks that traps divalent cations. At the same time, the crosslinked network is not a permanent structure because the monovalent ions in the surrounding environment will cause a reversible sol-gel transition and degrade the gel. Therefore, in my research the addition of suitable amount of Ca^{2+} in the cell medium is a good method to avoid structural collapse. We succeeded in preparing shear thinning solutions by incorporating cellulose

nanocrystals into alginate. Cellulose nanocrystals are known to be one of the most abundant natural materials on earth and could be used as biocompatible agents. The high crystallinity, elastic modulus, and tensile strength can contribute to their specific functions in changing properties of pure alginate. In addition, CNC introduced fibrous structures into the scaffolds to increase the mechanical strength and simulate the fibers in native extracellular matrices. During or after printing, the 3D scaffolds are exposed to external stimulus, yielding a physical or chemical gel network and providing further mechanical strength for handling. Ultimately, the aim of this research is to 3D bioprint human liver-mimetic structures using a bioink composed of alginate and CNC.

3.2 Materials and Methods

3.2.1 Materials

Pharm grade sodium alginate (PROTANAL LF 10/60 FT) with the amount of G residue of 60-70% was a product sample from FMC. Cellulose nanocrystals hydrolyzed from wood were donated from Professor Michael Tam's group. 3T3 fibroblast cell line and penicillin/ streptomycin were purchased from ATCC. Dulbecco's Modified Eagle's Medium (DMEM) was received from Lonza. Fetal bovine serum (FBS) was provided by Gibco. LIVE/DEAD viability/cytotoxicity kit (L-3224) was purchased from Life Technologies.

3.2.2 Ink preparation

The dry content of CNC was dispersed in Milli-Q water to prepare 2% (w/v), 4% (w/v), 6% (w/v), and 8% (w/v) CNC solutions followed by the addition of the same volume of 4% (w/v) alginate. Alginate were dissolved in Milli-Q water to prepare 2% (w/v), 4% (w/v), and 6% (w/v) pre-gel solutions. Seven formulations of inks were prepared with different proportions of Alginate/CNC as seen in Table 3.1. 20/40 were autoclaved at 121 ℃ for 20 min.

3.2.3 Cell culture and cell encapsulation

3T3 fibroblast were cultured in DMEM supplemented with 10% FBS and 100 unit/mL penicillin, 100 µg/mL streptomycin and maintained in a 5% CO_2 incubator at 37 ℃. 3T3 fibroblast were trypsinized

and counted. The initial cell viability was assessed using trypan-blue staining and then 3T3 fibroblast cells were resuspended in the bioinks at a density of 10^6 cells/mL.

3.2.4 Characterization of the hybrid bioinks

The rheological properties of the inks were analyzed using a Bohlin-CS Rheometer with a cup and bob geometry (C25, bob diameter of 25mm and gap width of 150μm). All measurements were tested at room temperature. The steady shear viscosities versus shear rate curves were determined under a constant rate mode. A strain sweep from 0.05% to 10% was performed at a frequency of 1 Hz to determine linear viscoelastic region (LVR). Subsequently, an optimized LVR strain of 0.1% was chosen for the oscillation frequency measurements performed from 0.1 to 10 Hz. The frequency sweeps were then used to define the elastic modulus (G') and the viscous modulus (G'').

3.2.5 3D printing

A FlashForge Creator Pro (FlashForge, China) was modified with a syringe-based extruder. The custom-made syringe pump extruder was designed by Brandon Justras and printed in PLA using the thermoplastic extruder on the FlashForge before its removal. The original thermoplastic extruder from the x-axis carriage was removed and replaced with the custom-made syringe holder where stepper motors were mounted. The stepper motor can be controlled by the same software that came with the printer. There is no need to modify the software to operate the printer, aside from settings corresponding to nozzle diameter, filament diameter, and extrusion temperature. Before bioprinting, the printer was wiped with 70% ethanol. Normal tape was used to fix the microscope cover glass on the printing platform, where the 3D constructs would be later laden. Liver-mimetic honeycomb models (spacing of 2.4 mm, wall thickness of 0.48 mm, and wall height of 1.2 mm) for printing were designed using Solidworks software and saved as STL format. This STL file was fabricated in ReplicatorG and sliced into 40-μm-thick layers to generate G-code instructions. The bioink-loaded glass syringe was equipped with a 32-gauge dispensable tip (EFD Nordson, USA) and fitted to the plastic syringe pump holder. Structures were performed at a print speed of 20 mm/s. After patterning the initial layer, the platform was degressively lowered in the z-axis to fabricate the next

layer, and repeated until the desired 3D scaffolds were generated. The printed constructs were then immediately immersed in 1% (w/v) $CaCl_2$ for 2 min, washed with serum-free DMEM, and then cultured in DMEM supplemented with 10%(v/v) FBS, 1% penicillin/ streptomycin, and 5 mM $CaCl_2$ in an incubator before analyzed with the LIVE/DEAD assays. Meanwhile, contrast samples were made without extrusion. 0.1 mL of 20/40 was placed on an autoclaved glass slide with 150 μm spacers, covered with a dialysis bag to make a flat surface, and then immersed in 1% (w/v) $CaCl_2$ for 2 min. The thin films were then cultured in the same condition as that of honeycomb constructs.

3.2.6 Scanning electron microscopy (SEM) analysis

The structure of the alginate-based hydrogels was imaged using a FE SEM (Zeiss Leo 1530). The test cylinder hydrogel samples (20/00 and 20/40) were first prepared in a custom-made teflon mold and immersed in a $CaCl_2$ bath to form consistently-sized samples. The crosslinked hydrogels were dropped into liquid nitrogen allowing them to freeze immediately. The frozen samples were lyophilized and then fractured into small pieces with a sharp blade. The samples were deposited on an aluminum holder and sputtered with a layer of gold in a sputter coater. The pore size and pore size distribution based on the SEM image was analyzed by ImageJ software.

3.2.7 Cell viability studies

A LIVE/DEAD viability/cytotoxicity kit was utilized to determine the cell viability within the unprinted and printed constructs over a period of 7 days. Calcein-AM/ethidium homodimer was diluted in serum-free DMEM with ratios of 1/2000 and 1/500 respectively. Samples were first washed with serum-free DMEM and then incubated in the staining solution for 2 hours. After staining, the samples were washed with serum-free medium for 10 min. Fluorescence microscope (Nikon Eclipse Ti-S) was used to image the live and dead cells within the constructs. A total six images from each sample were taken and analyzed using ImageJ software at day 0, 1, 3, 5, and 7. The cell viability was calculated by dividing the number of live cells by the total numbers of cells in the constructs.

3.3 Results and Discussion

3.3.1 Overview of the research process

The overview of the research process is illustrated in Fig. 3.1. The bioinks were prepared using different amounts of sodium alginate and cellulose nanocrystals. The ink formula were illustrated in Table 3.1. A rheometer was used to test the rheological properties, such as viscosity and modulus, of these formulations against constant rate and oscillation mode. Their printability and fidelity were later evaluated. All the constructs were printed with the same structural design, printing process, and crosslinking protocol. Considering their rheology and fidelity, 20/40 would be the ideal choice of the different formulations for 3D printing and biological studies. 20/40 was prepared in Milli-Q water at 65℃ and then autoclaved to sterilize. After cooled to room temperature, 3T3 fibroblasts were trypsinized and the cell suspensions were added to the bioink at a density of 10^6 cells/mL. A custom-made syringe extruder, which replaced the thermoplastic extruder from the x-axis carriage of a FlashForge 3D printer, was filled with the cell-suspended bioink and then used to extrude the pre-gel solution onto a cover glass layer-by-layer through a 32-gauge nozzle. Hexagon-based liver-mimetic 3D structures with a spacing of 2.4 mm, wall thickness of 0.48 mm, and wall height of 1.2 mm were further stabilized by crosslinking the alginate chains in a 2% (w/v) $CaCl_2$ bath for 2 min. Due to the high pressure on the bioinks at the nozzle wall, cells would experience high shear stress and cause some damages. Therefore, contrast samples (thin films) were fabricated by a template with an outer dimension of 26 mm×26 mm×0.15 mm. Due to the fact that ion exchange of the divalent and monovalent ions from the surrounding environments occurs in ionically crosslinked alginate hydrogels, the printed structures were immersed in $CaCl_2$ supplemented medium. Previous researches show that low concentrations of $CaCl_2$ fail to preserve the fidelity of the scaffolds for a long time, whereas medium supplemented with 5 mM or 10 mM $CaCl_2$ results in solid and durable structures. The 3T3 fibroblasts encapsulated films were immersed in $CaCl_2$ bath for 2 min and then incubated with printed honeycomb structures together in DEME supplemented with 10% (v/v) FBS, 100 unit/mL penicillin, 100 μg/mL streptomycin, and 5 mM $CaCl_2$ before analyzed with the LIVE/DEAD assay.

The cell media were also changed every second day. Molded cell-encapsulated hydrogel films and printed liver-mimetic structures were analyzed right after printing, then day 1, day 3, day 5, and day 7 to examine the effect of the printing process on cell viability.

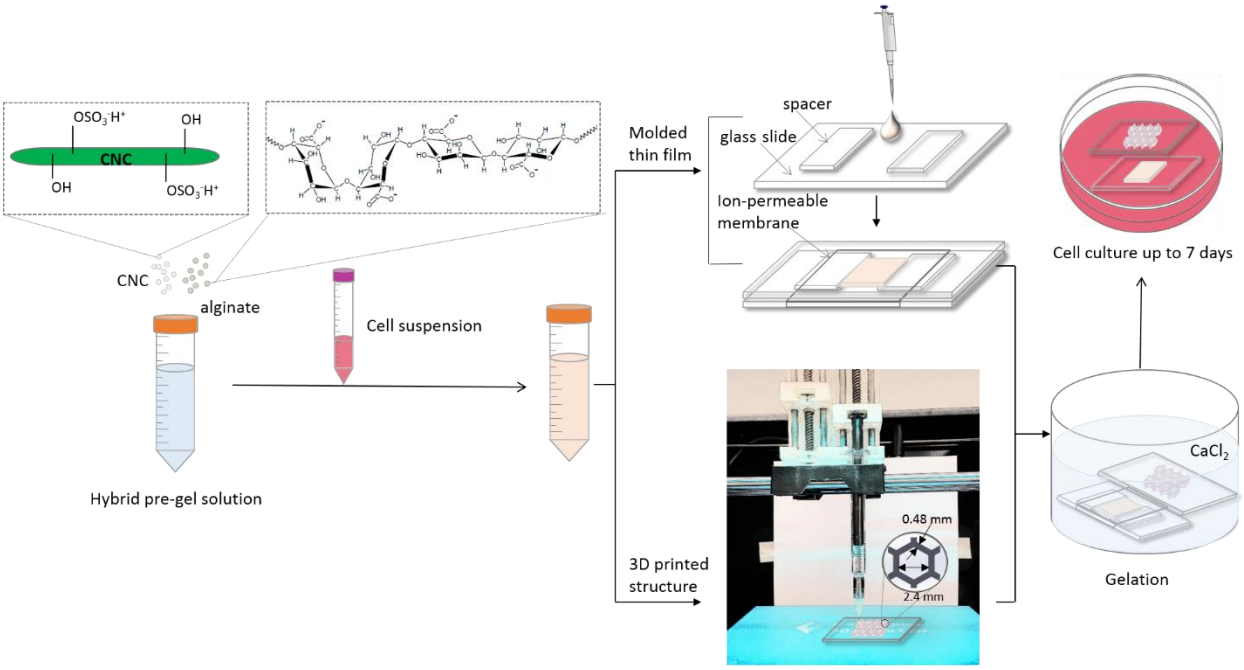

Figure 3.1: Schematic illustration of the fabrication process.

Table 3.1: Summary of ink formulations with different proportions of alginate and CNC.

Ink formula	Alginate/CNC (w/w)	Alginate (% w/v)	CNC (% w/v)	Water content (% w/v)
20/00	20:0	2	0	98
20/10	20:10	2	1	97
20/20	20:20	2	2	96
20/30	20:30	2	3	95
20/40	20:40	2	4	94
40/00	40:00	4	0	96
60/00	60:00	6	0	94

3.3.2 Characterization of the hybrid pre-gel solution

TEM image of CNC provided by Celluforce Inc. shows that the fibril's dimensions are 200-400 nm in length and 10-20 nm in diameter as shown in Fig. 3.2A. The surface charge density and surface area of CNC are 0.26 mmol/g and 500 m^2/g, respectively.

Rheological tests illustrate that the hybrid bioinks have significant differences when compared to pure alginate. Shear rate ramp tests performed on different formulations show that hybrid bioinks exhibit higher levels of viscosity at low shear rates when compared with pure alginate (Fig 3.2C and Fig. S1A). All hybrid bioinks show shear thinning behaviors as the incorporation of CNC increases the interactions between polymer chains. In a static state, alginate and CNC interlink together and are entangled randomly in the pre-gel solution, whereas upon shear stress on the solution, the entangled alginate would break and CNC would align in order to decrease the friction force between the two components leading to lower viscosity (Fig. 3.2B). It is also showed that at high shear rate, the addition of CNC did not have much effect on the viscosity of hybrid hydrogels with a constant alginate concentration. The flow curves of the 2% alginate series collapsed to one value at the high shear rate. However, for pure alginate by increasing concentration, the viscosity of increased over the whole shear rate range, but did not imply strong shear thinning behavior. When the concentration of alginate reached 6% (w/v), the viscosity was constant at low shear rates at a magnitude approximately lower than 20/40. It also illustrates that at high shear rates, the viscosity of the hybrid pre-gel solution was lower than pure alginate with high concentrations. After cells were in the bionics suspension at a concentration of 10^6 cells/mL, no significant changes in viscosity were observed (Fig. S2), which suggests that the mixture of cells does not change their rheological properties. In the shear-thinning region, the flow curve conforms to the well-known *"power-law"* model, $\eta = K\dot{\gamma}^{n-1}$, yielding a power-law index n of 0.23 for 20/40 as indicated in Fig. 3.2 C. According to n acquired, an estimated shear rate at the nozzle wall while printing can be obtained from an equation, $\dot{\gamma}_w = \frac{4Q}{\pi r^3}\left(\frac{3}{4} + \frac{1}{4n}\right)$, where Q is the volumetric flow rate and r is the nozzle radius. By substituting the value of n, Q, and r in the equation, we can conclude that the applied shear rate at the nozzle wall is approximately 300 s^{-1}, causing

the approximate viscosity of 0.5 Pa s during printing process. This value is roughly three orders of magnitude lower than those at smaller shear rates, enabling the bioink being extruded through a 100-μm-ID (inside diameter) nozzle readily with no clogging.

To increase the fidelity of the printed patterns, the modulus of the bioinks is another important rheological parameter that needs to be considered. The elastic modulus (G') and viscous modulus (G'') of different formulations are shown in Fig. 3D and Fig. S1B. Frequency sweeps at 0.1% strain reveal that all the modulus of hybrid bioinks increases with higher amount of CNC. The elastic modulus is smaller than the viscous modulus of pure alginate, indicating that 2% (w/v) alginate is liquid-like and not suitable for 3D printing. With the increasing concentration of alginate, both elastic and viscous modulus increased but elastic modulus is still lower than viscous modulus, suggesting that alginate with higher concentrations is still liquid-like and not ideal for 3D printing. However the addition of CNC in alginate changed the behavior of bioinks. For all the four formulations, the elastic modulus is larger than viscous modulus, which indicates that the hybrid bioinks are gel-like. There is more than two orders of magnitude increase in the modulus of 20/40, which indicates the increased rigidity of the 20/40. Moreover, no crossover of G' and G'' at low frequencies means that the bioink possesses a perpetual rigid gel network.

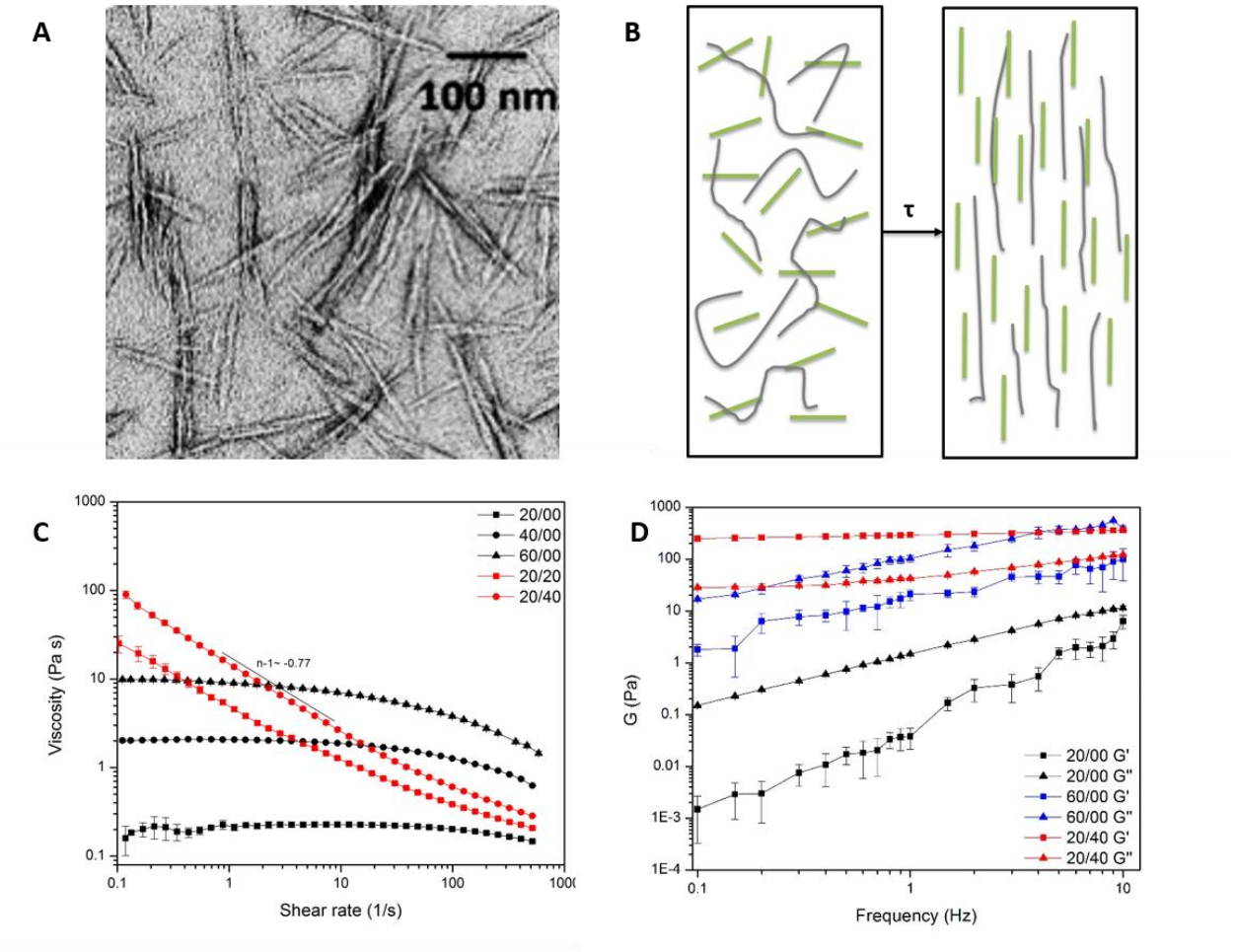

Figure 3.2: (A) TEM image of CNC. (B) Schematic illustration of interactions between alginate (grey) and CNC (green) in a static state and under shear stress (τ). In a static state (left), alginate and CNC are entangled in the hybrid solution randomly, while under shear stress (right), entangled alginate tends to break and CNC aligns in order. (C) Flow curves of five different bioink formulations, 20/00, 40/00, 60/00, 20/20, and 20/40 (as shown in table 1). (D) Elastic modulus (G') and viscous modulus (G'') of two different bioink formulations 20/00, 60/00, and 20/40 as a function of frequency.

3.3.3 Printability and fidelity of the bioinks

To evaluate the printability of the inks, the five formulations were studied. All of the structures were printed under the same printing protocol. The printed patterns were designed as liver-mimetic 3D honeycomb structures and the geometry of all the five printed structures is shown in Fig. 3.3. Pure alginate with a low shear viscosity gave a poor fidelity while printing. The printed pattern was a square-like shape and the printed size was larger than the designed size due to the spread and collapse of the ink as shown in Fig. 3.3A. With the increasing concentrations of added CNC, the viscosities increase (Fig. 3.2C) and the

geometry accords with the input design. For 20/10, 20/20, and 20/30, the inner hexagon parts were covered by a thin layer of inks while the periphery of all the structures retained their designed shape. These phenomena were attributed to the layer-by-layer printing technique, low viscosity of the inks, and crosslinking delay. The construct printed by 20/40 showed low deformation and relatively high accuracy. Light microscopy was performed on the printed structure by 20/40 showing that the printed inner hexagon structure became a circle with a diameter of 1.75 mm, smaller than the designed size of 2.4 mm. This needs to be further studied by developing the bioinks and crosslinking methods. Moreover, since the average diameter of a fibroblast cell is 10-15 μm and the diameter of the tips we used is 100 μm, the results reveal the potential use for cell studies. Taking all the factors into account, 20/40 would be an ideal bioink for cellular 3D printing.

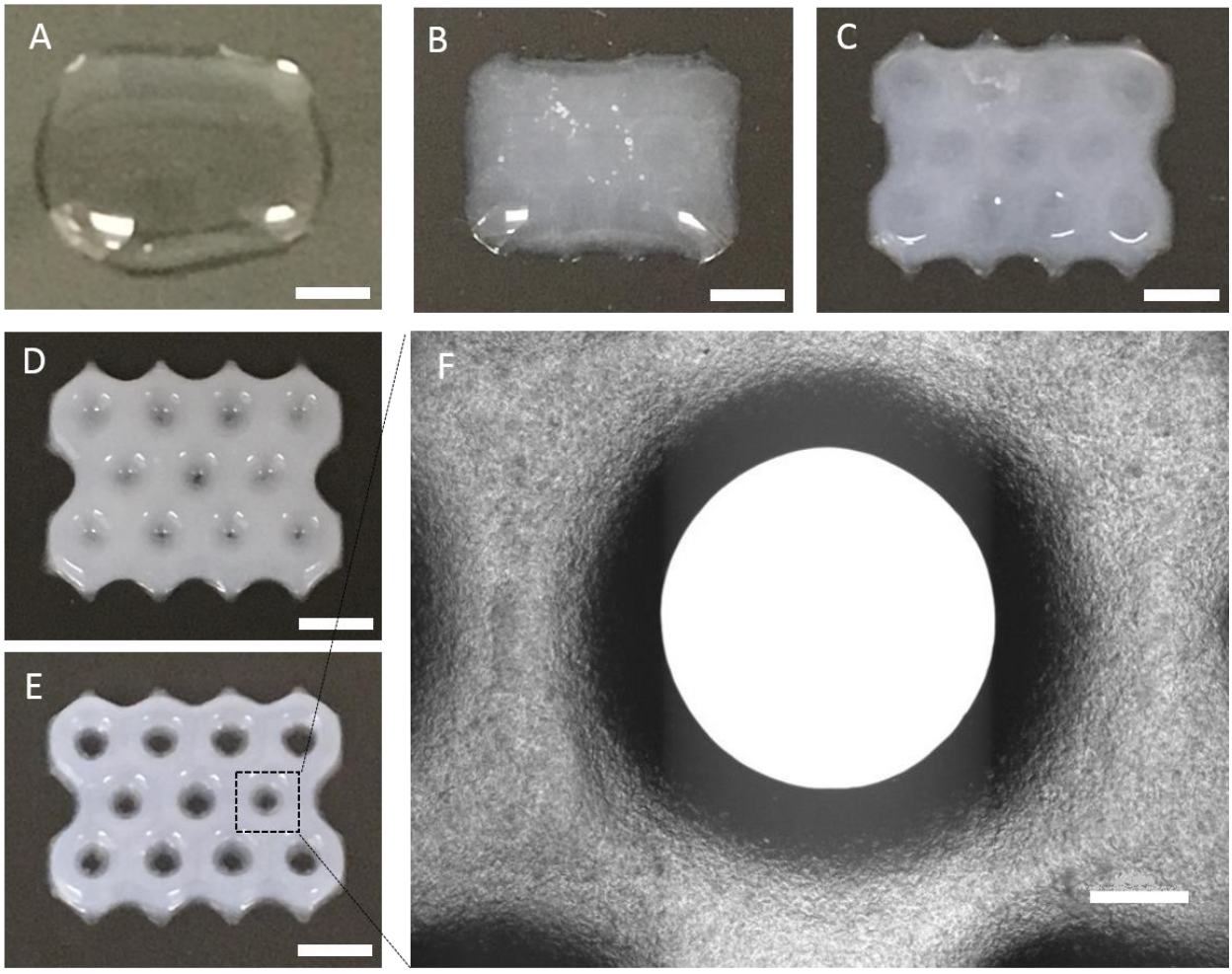

Figure 3.3: Photographs of 3D printed constructs with bioink formulations (A) 20/00, (B) 20/10, (C) 20/20,

(D) 20/30, (E) 20/40, and (F) the zoomed-in optical image of the construct printed by 20/40. Scale bar 5 mm in A-E and 500 μm in F.

3.3.4 SEM analysis of crosslinked hydrogels

SEM was employed to visualize the detailed structural features of 20/00 and 20/40. The samples were prepared in a custom-made mold and the crosslinked hydrogels were put in liquid nitrogen followed by freeze-drying immediately to avoid the deformation and collapse of the polymeric networks. However, after lyopilization the shrink of the pure alginate was more obvious than that of ALG-CNC. It can be deduced that the mechanical strength of the pure alginate was lower than ALG-CNC so that the network could not handle the freeze-drying procedure and some pores were collapsed and formed thick walls. The dry samples were then cut by a sharp blade into a thin sheet. Due to the insulation of the hydrogels, gold was coated on the surface of the samples. The SEM analysis of the pure alginate hydrogel showed a porous structure with microsized pores in the range of 7-178 μm. On the other hand, it showed that the incorporation of CNC in the alginate network led to more uniform pores. The hybrid hydrogels displayed highly porous and regular microstructure with a uniform pore size of 20 μm with parts of the walls being fractured. The smooth surface of the pore walls of the hybrid hydrogels confirmed the absence of CNC aggregation suggesting that all the CNC were suspended homogeneously in the alginate-based hydrogels matrix. CNC was bonded to the surface of alginate and formed a highly entangled network, resulting in improved toughness of the hybrid network. In addition, pore size and porosity are critical parameters in tissue engineering. Pores with large size can enhance nutrient mass transport and provide interstitial space for extracellular matrix deposition. Thus, the addition of CNC in alginate network improved the pore size and porosity, providing an ideal environment for cell activity.

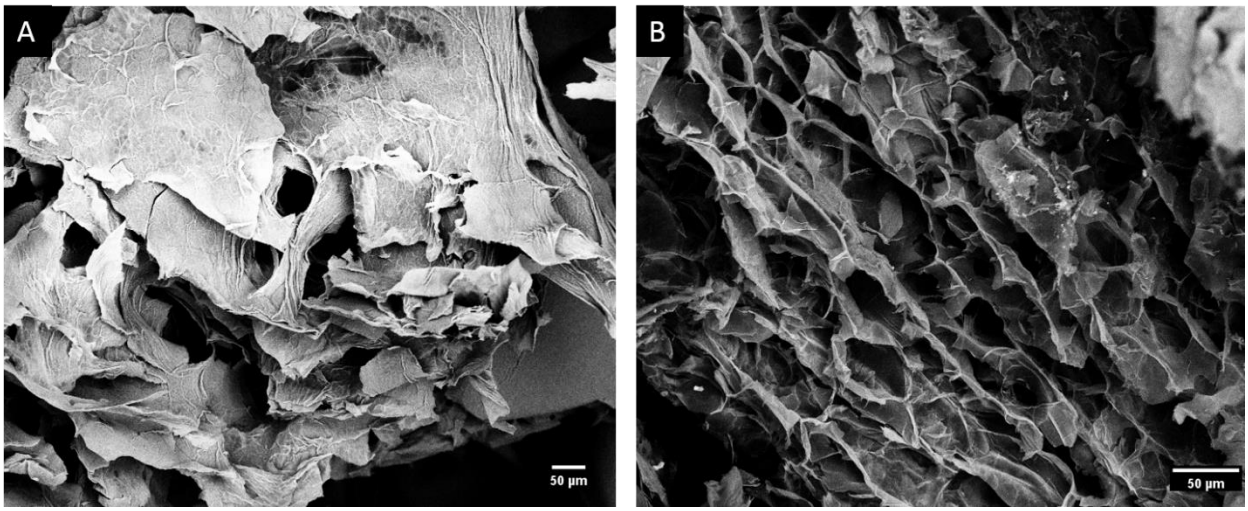

Figure 3.4: Scanning electron micrographs of the porous structure formed by calcium crosslinking (A) alginate (20/00) and (B) ALG-CNC (20/40) hydrogels.

3.3.5 Cell viability studies

To evaluate the biocompatibility of 20/40, 3T3 fibroblasts were suspended in the hybrid bioink and their viabilities were assessed over a 7-days period using the LIVE/DEAD cell-imaging assay. As controls, films made by the same cell-encapsulated bioinks without extruding through a 32-gauge nozzle were evaluated. Ten samples fabricated by two different protocols (five of each) were incubated in Ca^{2+} supplementing medium and imaged under fluorescence microscope. The initial cell viability (94.5±0.1%) measured after trypsinizing by using the trypan-blue exclusion method was significantly higher than those measured after being encapsulated into the bioinks, made into thin films, and then crosslinked (80.3±6.9%). This is attributed to stress applied on the cells during mixing process and Ca^{2+} crosslinking. No significant changes in the cell viability were observed in the high-resolution constructs (73.1±6.3%) when compared to molded structures immediately after printing. It demonstrates that flow-induced shear stress on the cells when passing through a 32-gauge nozzles does not influence the cell viability. The cell viability of the two groups' samples was analyzed with the following results 83.1±3.8% (1d), 73.0±4.9% (3d), 73.8±5.6% (5d), and 72.5±4.8% (7d) for thin film and 74.8±5.1% (1d), 74.5±6.3% (3d), 71.9±3.6% (5d), and 68.8±8.6% (7d) for honeycomb constructs (Fig. 3.5B). No significant differences between the molded structures and printed constructs were detected. Overall, the cell viability remained high during the experiment period,

demonstrating that the hybrid bioinks and the extrusion procedure have no side effect on the viability of the fibroblast cells. These results combined with the cell viability of printed constructs imply that this bioink is suitable for the 3D bioprinting of cells.

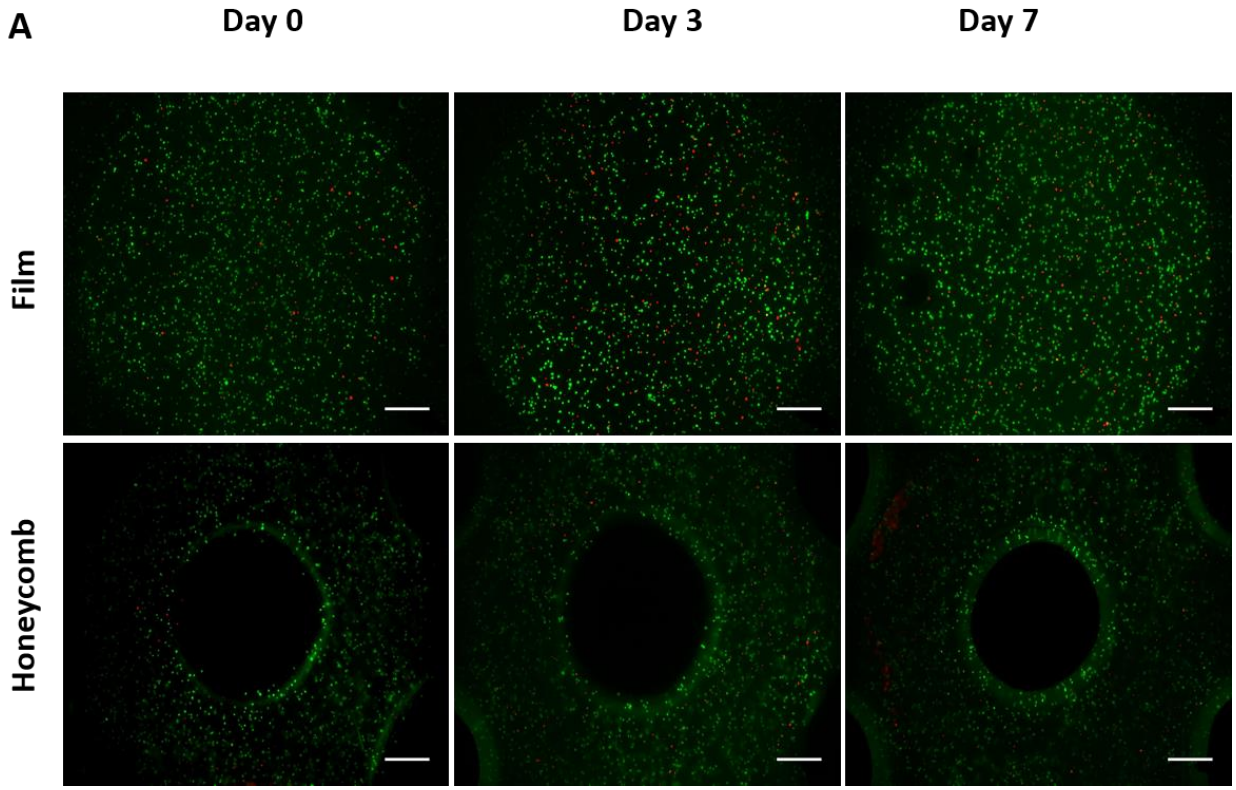

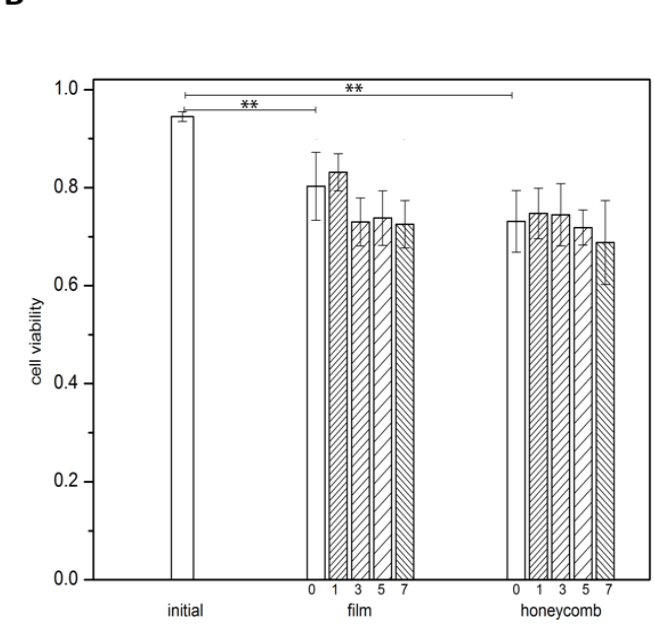

Figure 3.5: Viability evaluation of encapsulated fibroblasts using a fluorescence LIVE/DEAD assay. (A) Fluorescence images of fibroblasts encapsulated in molded films and printed honeycomb constructs fabricated with 20/40 bioink right after fabrication (day 0) and after culturing in cell medium for 3 days and 7 days. Live cells were stained with calcein-AM (green) and dead cells were stained with ethidium homodimer-1 (red). Scale bar 500 μm. (B) Cell viability (live cell populations/total cell populations) was obtained from the statistical analysis of the fluorescence images at various time points, before embedding (initial process), right after printing (day 0), and after culturing in cell medium for 1 day, 3 days, 5 days, and 7 days.

3.4 Conclusions

The new bioink described in this work was composed of alginate and cellulose nanocrystal. This hybrid pre-gel solution showed improved rheological performance, such as shear thinning behavior and high elastic modulus, which provided excellent printability and structural fidelity. The incorporation of functional nanomaterials was an effective approach to tune the rheological properties of the polymer solution. The shear thinning property of the hybrid bioink improved the control on the printability and fidelity of the 3D scaffolds. The 3D printed constructs were designed as hexagon-based liver-mimetic 3D structures. The cell viability of 3T3 fibroblasts in the printed scaffolds and molded films remained high over a 7-days period but was lower than the initial cell viability. It was found that the 3D constructs were biocompatible scaffolds for the cells and 3D printing process did not cause noticeable damage to the encapsulated cells. However, the mixing and the crosslinking procedure affected the cell viability. Overall, 3D printing is a technology platform that offers a novel approach for the engineering of tissues with complex and hierarchical structures.

Chapter 4: Summary and Future work

3D cell printing is an emerging technology that can fabricate physiological constructs and is expected to revolutionize the tissue engineering field. The materials used for 3D bioprinting should be able to withstand extrusion, able to retain their shape after deposition for long time periods, and biocompatible. Due to their intrinsic properties, hydrogels are good candidates for tissue engineering. This thesis aims at designing suitable bioinks for 3D printing, characterizing their properties and investigating their biocompatibility.

In **Chapter 2**, alginate hydrogels were incorporated with cellulose nanocrystals and their mechanical properties were examined. It was concluded that due to the high modulus and nanocrystal structure of CNC, it was able to increase the compression modulus of the hybrid hydrogel. Alginate was modified with AEMA to produce a photocrosslinkable polymer. Due to the ion exchange that occurs inside crosslinked alginate, the photo-curable alginate was more stable. Current date showed the success of binding carbon-carbon double bonds onto the backbone of alginate.

In **Chapter 3**, by controlling the composition of alginate and cellulose nanocystals, the rheological behavior can be tuned. It is suggested that the ideal hybrid ink composition for 3D printing among the formulations mentioned in the thesis is 2% (w/v) alginate with 4% (w/v) cellulose nanocrystals. Alginate was incorporated with cellulose nanocrystals before testing their rheology. It was concluded that with the increasing concentration of CNC, the shear thinning behavior was stronger and the modulus of the hybrid pre-gel solution was increased as well. The crystalline structure of cellulose nanocrystals and hydrogen bonding between alginate and CNC yielded a viscoelastic ink that could flow through 100 μm nozzles. With the described system, it was shown that the shear thinning behavior enabled the printability of the pre-gel solution and high modulus allowed the fidelity of the printed constructs. Finally, cell viability was investigated. It was shown that 3D alginate-CNC scaffolds fabricated by 3D printing supported 3T3 fibroblasts. The loss of cell viability was mainly contributed to mixing and crosslinking procedure. Therefore new crosslinking methods and gentle operation are recommended to improve cell viability. Thus

with this study, a new opportunity for printing complex physiological tissue constructs is opened up.

From the research on 3D printing of hybrid hydrogels described in this thesis, several recommendations for future work can be made.

(1) Printability and fidelity are the two most important parameters in 3D printing. This research further emphasizes this point where despite the success of the 3D printing, the fidelity of the construct needs to be improved. Deformation of the engineered structures was observed because of the time delay between printing and crosslinking. There are two ways to solve this problem. The first one is to print the constructs on a paper where $CaCl_2$ solution can flow continuously to allow the alginate crosslinking occuring during printing process. In this method, the paper needs to be flat whilst in $CaCl_2$ solution and be able to bind to printed structures firmly during printing. An alternative method is to modify the alginate to form photoinduced polymers. Previous research has shown that metharylated alginate (AEMA) can be photocrosslinked when exposed to UV light and AEMA can support cell activities due to its biodegradable ester groups. However, UV light might kill the encapsulated cells in the tissue matrices, so conventional photoinitiators cannot be used. Due to the cells inside the hybrid hydrogels, infrared or near-infrared induced photoinitiators are good candidates for tissue engineering. Future work on photinitiators and their effects on cell viability should be conducted.

(2) By virtue of the effect of surface functionalities on the cell behavior, peptide motifs should be introduced to the surface of alginate or collagen and gelatin can be incorporated into the hybrid pre-gel solution to provide platforms for cell migration, differentiation, and proliferation. Gelatin is a thermal-responsive hydrogel which will liquefies at 37℃ and leaves macroporous structures in the tissue scaffolds, so the incorporation of gelatin alone is not ideal for tissue scaffolds. Previous research illustrates that GelMA helped improve the migration and adhesion of the cells due to the presence of integrin-binding motifs and matrix metalproteinase sensitive groups. In addition, the incorporation of GelMA can strengthen the scaffolds by chemical crosslinking between AEMA and GelMA. A mixture of gelatin and GelMA can also be incorporated into the hybrid solution together

to introduce porous structures for nutrients delivery and integrin-binding sites for improved cell behavior.

(3) Incorporating functional nanomaterials, such as conductive cellulose nanocrystals and graphene derivatives, into alginate matrix can be an effective approach to reinforce the mechanical properties of the printed 3D scaffolds and introduce the electrical conductivity to the matrix. The cell behaviors, including cell migration and adhesion, DNA synthesis, and protein secretion, have been shown to change with electrical stimulus. Neurons are able to use electrochemical signal in the mV range to regulate cellular functions, and promote the development of neural tissue. Efforts will be devoted to the development of conductive CNC and reduced graphene oxide (rGO). Normally, conductive CNC and rGO are not soluble in water, which makes preparation in ink difficult. Novel methods of modifying CNC and GO will be conducted in the future to produce water-soluble conductive materials. Meanwhile, it is recommended to investigate the mechanical properties of hybrid materials that can help maintain the mechanical strength of the designed tissue or organs while tuning the concentrations of different materials.

(4) Only one cell line was used to study cell viability in this study, which does not reflect the phenomenon of the human body where multiple-cell lines coexist in one tissue. In order to highly mimic human tissues, multiple cell lines will be introduced in the bioinks to print complex constructs. The main goal of my research is to print liver structures and thus hepatocytes will be utilized in addition to the fibroblasts. Confocal microscope will be used to investigate the cellular interactions between cell-cell and cell-matrix. Cell viability will also be studied to test the biocompatibility of the bioinks. In order to print two or more cell lines, a multi-extruder is needed to dispense different bioinks, which means that a remodification of the 3D printer is required.

References

(1) Fedorovich, N. E.; Alblas, J.; Wijn, J. R. DE; Hennink, W. E.; Verbout, A. J.; Dhert, W. J. A. Hydrogels as Extracellular Matrices for Skeletal Tissue Engineering: State-of-the-Art and Novel Application in Organ Printing. *Tissue Eng.* **2007**, *13*, 1905–1925.

(2) Gross, B. C.; Erkal, J. L.; Lockwood, S. Y.; Chen, C.; Spence, D. M. Evaluation of 3D Printing and Its Potential Impact on Biotechnology and the Chemical Sciences. *Anal. Chem.* **2014**, *86*, 3240–3253.

(3) Berman, B.; Zarb, F. G.; Hall, W. 3-D Printing: The New Industrial Revolution. *Bus. Horiz.* **2012**, *55*, 155–162.

(4) Gibson, I.; Rosen, D. *Additive Manufacturing Technologies*; 2015.

(5) Guvendiren, M.; Molde, J.; Soares, R. M. D.; Kohn, J. Designing Biomaterials for 3D Printing. *ACS Biomater. Sci. Eng.* **2016**, *2*, 1678–1683.

(6) Jang, J.; Yi, H.; Cho, D. 3D Printed Tissue Models: Present and Future. *ACS Biomater. Sci. Eng.* **2016**, *2*, 1722–1731.

(7) Billiet, T.; Vandenhaute, M.; Schelfhout, J.; Vlierberghe, S. Van; Dubruel, P. A Review of Trends and Limitations in Hydrogel-Rapid Prototyping for Tissue Engineering. *Biomaterials* **2012**, *33*, 6020–6041.

(8) Landers, R.; Pfister, A.; John, H. Fabrication of Soft Tissue Engineering Scaffolds by Means of Rapid Prototyping Techniques. *J. Mater. Sci.* **2002**, *37*, 3107–3116.

(9) Wüst, S.; Müller, R.; Hofmann, S. Controlled Positioning of Cells in Biomaterials—approaches towards 3D Tissue Printing. *J. Funct. Biomater.* **2011**, *2*, 119–154.

(10) Murphy, S. V; Atala, A. 3D Bioprinting of Tissues and Organs. *Nat. Biotechnol.* **2014**, *32*, 773–785.

(11) Tumbleston, J. R.; Shirvanyants, D.; Ermoshkin, N.; Janusziewicz, R.; Johnson, A. R.; Kelly, D.; Chen, K.; Pinschmidt, R.; Rolland, J. P.; Ermoshkin, A.; *et al.* Continuous Liquid Interface Production of 3D Objects. *Science* **2015**, *347*, 1349–1352.

(12) Sachlos, E.; Czernuszka, J. T. Making Tissue Engineering Scaffolds Work. Review on the Application of Solid Freeform Fabrication Technology to the Production of Tissue Engineering Scaffolds. *Eur. Cells Mater.* **2003**, *5*, 29–40.

(13) Nerem, R. M.; Sambanis, A. Tissue Engineering: From Biology to Biological Substitutes. *Tissue Eng.* **1995**, *1*, 3–13.

(14) Khademhosseini, A.; Langer, R.; Borenstein, J.; Vacanti, J. P. Microscale Technologies for Tissue Engineering and Biology. *PNAS* **2006**, *103*, 2480–2487.

(15) Hutmacher, D. W.; Sittinger, M.; Risbud, M. V. Scaffold-Based Tissue Engineering: Rationale for Computer-Aided Design and Solid Free-Form Fabrication Systems. *Trends Biotechnol.* **2004**, *22*, 354–362.

(16) Yang, S.; Leong, K.; Du, Z.; Chua, C. The Design of Scaffolds for Use in Tissue Engineering. Part I. Traditional Factors. *Tissue Eng.* **2001**, *7*, 679–689.

(17) Melchels, F. P. W.; Domingos, M. A. N.; Klein, T. J.; Malda, J.; Bartolo, P. J.; Hutmacher, D. W. Additive Manufacturing of Tissues and Organs. *Prog. Polym. Sci.* **2012**, *37*, 1079–1104.

(18) Abbott, A. Biology's New Dimension. *Nature* **2003**, *424*, 870–872.

(19) Pampaloni, F.; Reynaud, E. G.; Stelzer, E. H. K. The Third Dimension Bridges the Gap between Cell Culture and Live Tissue. *Nat. Rev. Mol. Cell Biol.* **2007**, *8*, 839–845.

(20) Ghaemmaghami, A. M.; Hancock, M. J.; Harrington, H.; Kaji, H.; Khademhosseini, A. Biomimetic Tissues on a Chip for Drug Discovery. *Drug Discov. Today* **2012**, *17*, 173–181.

(21) Griffith, L. G.; Swartz, M. A. Capturing Complex 3D Tissue Physiology in Vitro. *Nat. Rev. Mol. Cell Biol.* **2006**, *7*, 211–224.

(22) Place, E. S.; Evans, N. D.; Stevens, M. M. Complexity in Biomaterials for Tissue Engineering. *Nat. Mater.* **2009**, *8*, 457–470.

(23) Yang, S.; Leong, K.; Du, Z.; Chua, C. The Design of Scaffolds for Use in Tissue Engineering. Part II. Rapid Prototyping Techniques. *Tissue Eng.* **2002**, *8*, 1–11.

(24) Discher, D. E.; Mooney, D. J.; Zandstra, P. W. Growth Factors, Matrices, and Forces Combine and Control Stem Cells. *Science* **2009**, *324*, 1673–1678.

(25) Eisenbarth, E. Biomaterials for Tissue Engineering. *Adv. Eng. Mater.* **2007**, *9*, 1051–1060.

(26) Drury, J. L.; Mooney, D. J. Hydrogels for Tissue Engineering: Scaffold Design Variables and Applications. *Biomaterials* **2003**, *24*, 4337–4351.

(27) Griffith, L. G.; Naughton, G. Tissue Engineering—current Challenges and Expanding Opportunities. *Science* **2002**, *295*, 1009–1014.

(28) Jen, A. C.; Wake, M. C.; Mikos, A. G. Review: Hydrogels for Cell Immobilization. *Biotechnol. Bioeng.* **1996**, *50*, 357–364.

(29) Grigore, A.; Sarker, B.; Fabry, B.; Boccaccini, A. R.; Detsch, R. Behavior of Encapsulated MG-63 Cells in RGD and Gelatine-Modified Alginate Hydrogels. *Tissue Eng. Part A* **2014**, *20*, 2140–2150.

(30) Place, E. S.; George, J. H.; Williams, C. K.; Stevens, M. M. Synthetic Polymer Scaffolds for Tissue Engineering. *Chem. Soc. Rev.* **2009**, *38*, 1139–1151.

(31) Tibbitt, M. W.; Anseth, K. S. Hydrogels as Extracellular Matrix Mimics for 3D Cell Culture. *Biotechnol. Bioeng.* **2009**, *103*, 655–663.

(32) Lutolf, M. P.; Hubbell, J. a. Synthetic Biomaterials as Instructive Extracellular Microenvironments for Morphogenesis in Tissue Engineering. *Nat. Biotechnol.* **2005**, *23*, 47–55.

(33) Jin, G.; Li, K. The Electrically Conductive Scaffold as the Skeleton of Stem Cell Niche in Regenerative Medicine. *Mater. Sci. Eng. C* **2014**, *45*, 671–681.

(34) Borriello, A.; Guarino, V.; Schiavo, L.; Alvarez-Perez, M. A.; Ambrosio, L. Optimizing PANi Doped Electroactive Substrates as Patches for the Regeneration of Cardiac Muscle. *J. Mater. Sci. Mater. Med.* **2011**, *22*, 1053–1062.

(35) Shin, S. R.; Jung, S. M.; Zalabany, M.; Kim, K.; Zorlutuna, P.; Kim, S.; Nikkhah, M.; Khabiry, M.; Azize, M.; Kong, J.; *et al.* Carbon-Nanotube-Embedded Hydrogel Sheets for Engineering Cardiac Constructs and Bioactuators. *ACS Nano* **2013**, *7*, 2369–2380.

(36) Dvir, T.; Timko, B. P.; Brigham, M. D.; Naik, S. R.; Karajanagi, S. S.; Levy, O.; Jin, H.; Parker, K. K.; Langer, R.; Kohane, D. S. Nanowired Three-Dimensional Cardiac Patches. *Nat. Nanotechnol.* **2011**, *6*, 1–6.

(37) Hoffman, A. S. Hydrogels for Biomedical Applications. *Adv. Drug Deliv. Rev.* **2012**, *64*, 18–23.

(38) Lee, K. Y.; Rowley, J. A.; Eiselt, P.; Moy, E. M.; Bouhadir, K. H.; Mooney, D. J. Controlling Mechanical and Swelling Properties of Alginate Hydrogels Independently by Cross-Linker Type and Cross-Linking Density. *Macromolecules* **2000**, *33*, 4291–4294.

(39) Hennink, W. E.; Nostrum, C. F. Van. Novel Crosslinking Methods to Design Hydrogels. *Adv. Drug Deliv. Rev.* **2012**, *64*, 223–236.

(40) Chen, G.; Ushida, T.; Tateishi, T. Scaffold Design for Tissue Engineering. *Macromol. Biosci.* **2002**, *2*, 67–77.

(41) Hansen, C. J.; Wu, W.; Toohey, K. S.; Sottos, N. R.; White, S. R.; Lewis, J. A. Self-Healing Materials with Interpenetrating Microvascular Networks. *Adv. Mater.* **2009**, *21*, 4143–4147.

(42) Wu, W.; Deconinck, A.; Lewis, J. A. Omnidirectional Printing of 3D Microvascular Networks. *Adv. Mater.* **2011**, *23*, 178–183.

(43) Kolesky, D. B.; Truby, R. L.; Gladman, A. S.; Busbee, T. A.; Homan, K. A.; Lewis, J. A. 3D Bioprinting of Vascularized, Heterogeneous Cell-Laden Tissue Constructs. *Adv. Mater.* **2014**, *26*, 3124–3130.

(44) Malda, J.; Visser, J.; Melchels, F. P.; Jüngst, T.; Hennink, W. E.; Dhert, W. J. A.; Groll, J.; Hutmacher, D. W. Engineering Hydrogels for Biofabrication. *Adv. Mater.* **2013**, *25*, 5011–5028.

(45) Robert, B.; Iii, A. B.; Shepherd, R. F.; Hanson, J. N.; Nuzzo, R. G.; Wiltzius, P.; Lewis, J. A. Direct-Write Assembly of 3D Hydrogel Scaffolds for Guided Cell Growth. *Adv. Mater.* **2009**, *21*, 1–4.

(46) Shepherd, J. N. H.; Parker, S. T.; Shepherd, R. F.; Gillette, M. U.; Lewis, J. A.; Nuzzo, R. G. 3D Microperiodic Hydrogel Scaffolds for Robust Neuronal Cultures. *Adv. Funct. Mater.* **2011**, *21*, 47–54.

(47) Shin, S. R.; Bae, H.; Cha, J. M.; Mun, J. Y.; Chen, Y.; Tekin, H.; Shin, H.; Farshchi, S.; Dokmeci, M. R.; Tang, S.; *et al.* Carbon Nanotube Reinforced Hybrid Microgels as Scaffold Materials for Cell Encapuslation. *ACS Nano* **2012**, *6*, 362–372.

(48) Kojima, C.; Suehiro, T.; Watanabe, K.; Ogawa, M.; Fukuhara, A.; Nishisaka, E.; Harada, A.; Kono, K.; Inui, T.; Magata, Y. Doxorubicin-Conjugated Dendrimer/collagen Hybrid Gels for Metastasis-Associated Drug Delivery Systems. *Acta Biomater.* **2013**, *9*, 5673–5680.

(49) Hadi, M. F.; Sander, E. A.; Ruberti, J. W.; Barocas, V. H. Simulated Remodeling of Loaded Collagen Networks via Strain-Dependent Enzymatic Degradation and Constant-Rate Fiber Growth. *Mech. Mater.* **2012**, *44*, 72–82.

(50) Yeo, M. G.; Lee, J. S.; Chun, W.; Kim, G. H. An Innovative Collagen-Based Cell-Printing Method for Obtaining Human Adipose Stem Cell-Laden Structures Consisting of Core-Sheath Structures for Tissue Engineering. *Biomacromolecules* **2016**, *17*, 1365–1375.

(51) Kolesky, D. B.; Homan, K. A.; Skylar-Scott, M. A.; Lewis, J. A. Three-Dimensional Bioprinting of Thick Vascularized Tissues. *Proc. Natl. Acad. Sci. U. S. A.* **2016**, *113*, 3179–3184.

(52) Gomez-Guillen, M. C.; Gimenez, B.; Lopez-Caballero, M. E.; Montero, M. P. Functional and Bioactive Properties of Collagen and Gelatin from Alternative Sources: A Review. *Food Hydrocoll.* **2011**, *25*, 1813–1827.

(53) Zhao, Y.; Yao, R.; Ouyang, L.; Ding, H.; Zhang, T.; Zhang, K.; Cheng, S.; Sun, W. Three-Dimensional Printing of Hela Cells for Cervical Tumor Model in Vitro. *Biofabrication* **2014**, *6*, 35001.

(54) Cha, C.; Shin, S. R.; Gao, X.; Annabi, N.; Dokmeci, M. R.; Tang, X.; Khademhosseini, A. Controlling Mechanical Properties of Cell-Laden Hydrogels by Covalent Incorporation of Graphene Oxide. *Small* **2014**, *10*, 514–523.

(55) Ahmed, T. A. E.; Dare, E. V.; Hincke, M. Fibrin: A Versatile Scaffold for Tissue Engineering Applications. *Tissue Eng. Part B* **2008**, *14*, 199–215.

(56) Fisher, J. P. *Advances in Experimental Medicine and Biology*; 2005; Vol. 585.

(57) Geng, L.; Feng, W.; Hutmacher, D. W.; Wong, Y. S.; Loh, H. T.; Fuh, J. Y. H. Direct Writing of Chitosan Scaffolds Using a Robotic System. *Rapid Prototyp. J.* **2005**, *11*, 90–97.

(58) Rodell, C. B.; MacArthur, J. W.; Dorsey, S. M.; Wade, R. J.; Wang, L. L.; Woo, Y. J.; Burdick, J. A. Shear-Thinning Supramolecular Hydrogels with Secondary Autonomous Covalent Crosslinking to Modulate Viscoelastic Properties in Vivo. *Adv. Funct. Mater.* **2015**, *25*, 636–644.

(59) Samavedi, S.; Whittington, A. R.; Goldstein, A. S. Calcium Phosphate Ceramics in Bone Tissue Engineering: A Review of Properties and Their Influence on Cell Behavior. *Acta Biomater.* **2013**, *9*, 8037–8045.

(60) Yuan, H.; Fernandes, H.; Habibovic, P.; de Boer, J.; Barradas, A. M. C.; de Ruiter, A.; Walsh, W. R.; van Blitterswijk, C. A.; de Bruijn, J. D. Osteoinductive Ceramics as a Synthetic Alternative to Autologous Bone Grafting. *Proc. Natl. Acad. Sci. U. S. A.* **2010**, *107*, 13614–13619.

(61) Michna, S.; Wu, W.; Lewis, J. A. Concentrated Hydroxyapatite Inks for Direct-Write Assembly of 3-D Periodic Scaffolds. *Biomaterials* **2005**, *26*, 5632–5639.

(62) Lewis, J. A.; Smay, J. E.; Stuecker, J.; Cesarano, J. Direct Ink Writing of Three-Dimensional Ceramic Structures. *J. Am. Ceram. Soc.* **2006**, *89*, 3599–3609.

(63) Armstrong, J. P. K.; Burke, M.; Carter, B. M.; Davis, S. A.; Perriman, A. W. 3D Bioprinting Using a Templated Porous Bioink. *Adv. Healthc. Mater.* **2016**, *5*, 1724–1730.

(64) Shin, S. R.; Aghaei-Ghareh-Bolagh, B.; Dang, T. T.; Topkaya, S. N.; Gao, X.; Yang, S. Y.; Jung, S. M.; Oh, J. H.; Dokmeci, M. R.; Tang, X.; *et al.* Cell-Laden Microengineered and Mechanically Tunable Hybrid Hydrogels of Gelatin and Graphene Oxide. *Adv. Mater.* **2013**, *25*, 6385–6391.

(65) Smay, J. E.; Gratson, G. M.; Shepherd, R. F.; Cesarano, J.; Lewis, J. A. Colloidal Inks for Directed Assembly of 3-D Periodic Structures. *Adv. Mater.* **2002**, *18*, 1279–1283.

(66) Smay, J. E.; Cesarano, J.; Lewis, J. A. Colloidal Inks for Directed Assembly of 3-D Periodic Structures. *Langmuir* **2002**, *18*, 5429–5437.

(67) Duoss, E. B.; Twardowski, M.; Lewis, J. A. Sol-Gel Inks for Direct-Write Assembly of Functional Oxides. *Adv. Mater.* **2007**, *19*, 3485–3489.

(68) Xu, M.; Lewis, J. A. Phase Behavior and Rheological Properties of Polyamine-Rich Complexes for Direct-Write Assembly. *Langmuir* **2007**, *23*, 12752–12759.

(69) Lewis, J. A. Direct Ink Writing of 3D Functional Materials. *Adv. Funct. Mater.* **2006**, *16*, 2193–2204.

(70) Barnes, H. A.; Hutton, J. F.; Walters, F. R. S. K. *An Introduction to Rheology*; Elsevier: The Nertherlands, 1989; Vol. 3.

(71) Chen, K. L.; Mylon, S. E.; Elimelech, M.; Pennsyl, V. Enhanced Aggregation of Alginate-Coated Iron Oxide (Hematite) Nanoparticles in the Presence of Calcium, Strontium, and Barium Cations. *Langmuir* **2007**, *23*, 5920–5928.

(72) Kuo, C. K.; Ma, P. X. Ionically Crosslinked Alginate Hydrogels as Scaffolds for Tissue Engineering: Part 1. Structure, Gelation Rate and Mechanical Properties. *Biomaterials* **2001**, *22*, 511–521.

(73) Smidsrød, O.; Skjåk-Braek, G. Alginate as Immobilization Matrix for Cells. *Trends Biotechnol.* **1990**, *8*, 71–78.

(74) Rowley, J. A.; Madlambayan, G.; Mooney, D. J. Alginate Hydrogels as Synthetic Extracellular Matrix Materials. *Biomaterials* **1999**, *20*, 45–53.

(75) Augst, A. D.; Kong, H. J.; Mooney, D. J. Alginate Hydrogels as Biomaterials. *Macromol. Biosci.* **2006**, *6*, 623–633.

(76) Jeon, O.; Bouhadir, K. H.; Mansour, J. M.; Alsberg, E. Photocrosslinked Alginate Hydrogels with Tunable Biodegradation Rates and Mechanical Properties. *Biomaterials* **2009**, *30*, 2724–2734.

(77) Yang, J.; Xie, Y.; He, W. Research Progress on Chemical Modification of Alginate: A Review. *Carbohydr. Polym.* **2011**, *84*, 33–39.

(78) Domingues, R. M. A.; Gomes, M. E.; Reis, R. L. The Potential of Cellulose Nanocrystals in Tissue Engineering Strategies. *Biomacromolecules* **2014**, *15*, 2327–2346.

(79) Lu, P.; Hsieh, Y. Preparation and Properties of Cellulose Nanocrystals: Rods, Spheres, and Network. *Carbohydr. Polym.* **2010**, *82*, 329–336.

(80) Habibi, Y.; Lucia, L. A.; Rojas, O. J. Cellulose Nanocrystals: Chemistry, Self-Assembly, and Applications. *Chem. Rev.* **2010**, *110*, 3479–3500.

(81) Huq, T.; Salmieri, S.; Khan, A.; Khan, R. A.; Le, C.; Riedl, B.; Fraschini, C.; Bouchard, J.; Uribe-calderon, J.; Kamal, M. R.; *et al.* Nanocrystalline Cellulose (NCC) Reinforced Alginate Based Biodegradable Nanocomposite Film. *Carbohydr. Polym.* **2012**, *90*, 1757–1763.

(82) Lam, E.; Male, K. B.; Chong, J. H.; Leung, A. C. W.; Luong, J. H. T. Applications of Functionalized and Nanoparticle-Modified Nanocrystalline Cellulose. *Trends Biotechnol.* **2012**, *30*, 283–290.

(83) Ahmed, M.; Azizi, S.; Alloin, F.; Dufresne, A. Review of Recent Research into Cellulosic Whiskers, Their Properties and Their Application in Nanocomposite Field. *Biomacromolecules* **2005**, *6*, 612–626.

(84) Hubbe, M. A.; Rojas, O. J.; Lucia, L. A.; Sain, M. Cellulosic Nanocomposites: A Review. *Bioresources* **2008**, *3*, 929–980.

(85) Lin, N.; Huang, J.; Dufresne, A. Preparation, Properties and Applications of Polysaccharide Nanocrystals in Advanced Functional Nanomaterials: A Review. *Nanoscale* **2012**, *4*, 3274–3294.

(86) Lin, N.; Dufresne, A. Nanocellulose in Biomedicine : Current Status and Future Prospect. *Eur. Polym. J.* **2014**, *59*, 302–325.

(87) Moon, R. J.; Martini, A.; Nairn, J.; Youngblood, J.; Martini, A.; Nairn, J. Cellulose Nanomaterials Review: Structure, Properties and Nanocomposites. *Chem. Soc. Rev.* **2011**, *40*, 3941–3994.

(88) Yang, X.; Cranston, E. D. Chemically Cross-Linked Cellulose Nanocrystal Aerogels with Shape Recovery and Superabsorbent Properties. *Chem. Mater.* **2014**, *26*, 6016–6025.

(89) Ureña-Benavides, E. E.; Ao, G.; Davis, V. A.; Kitchens, C. L. Rheology and Phase Behavior of Lyotropic Cellulose Nanocrystal Suspensions. *Macromolecules* **2011**, *44*, 8990–8998.

(90) Wu, X.; Chabot, V. L.; Kim, B. K.; Yu, A.; Berry, R. M.; Tam, K. C. Cost-Effective and Scalable Chemical Synthesis of Conductive Cellulose Nanocrystals for High-Performance Supercapacitors. *Electrochim. Acta* **2014**, *138*, 139–147.

(91) Mattoso, L. H. C.; Medeiros, E. S.; Baker, D. A.; Avloni, J.; Wood, D. F.; Orts, W. J. Electrically Conductive Nanocomposites Made from Cellulose Nanofibrils and Polyaniline. *J. Nanosci. Nanotechnol.* **2009**, *9*, 2917–2922.

(92) Khan, S.; UI-Islam, M.; Ullah, M. W.; Kim, Y.; Park, J. K. Synthesis and Characterization of a Novel Bacterial Cellulose-poly(3.4-Ethylenedioxythiophene)-Poly(styrene Sulfonate)composite for Use in Biomedical Applications. *Cellulose* **2015**, *22*, 2141–2148.

(93) Berg, O. Van Den; Schroeter, M.; Capadona, R.; Weder, C. Nanocomposites Based on Cellulose Whiskers and (Semi)conducting Conjugated Polymers. *J. Mater. Chemsitry* **2007**, *17*, 2746–2753.

(94) Dugan, J. M.; Gough, J. E.; Eichhorn, S. J. Directing the Morphology and Differentiation of Skeletal Muscle Cells Using Oriented Cellulose Nanowhiskers. *Biomacromolecules* **2010**, *11*, 2498–2504.

(95) Shackelford, J. F. *Introduction to Materials Science for Engineers*; 2001.

Appendix A: Supplementary date for characterization of hybrid hydrogel

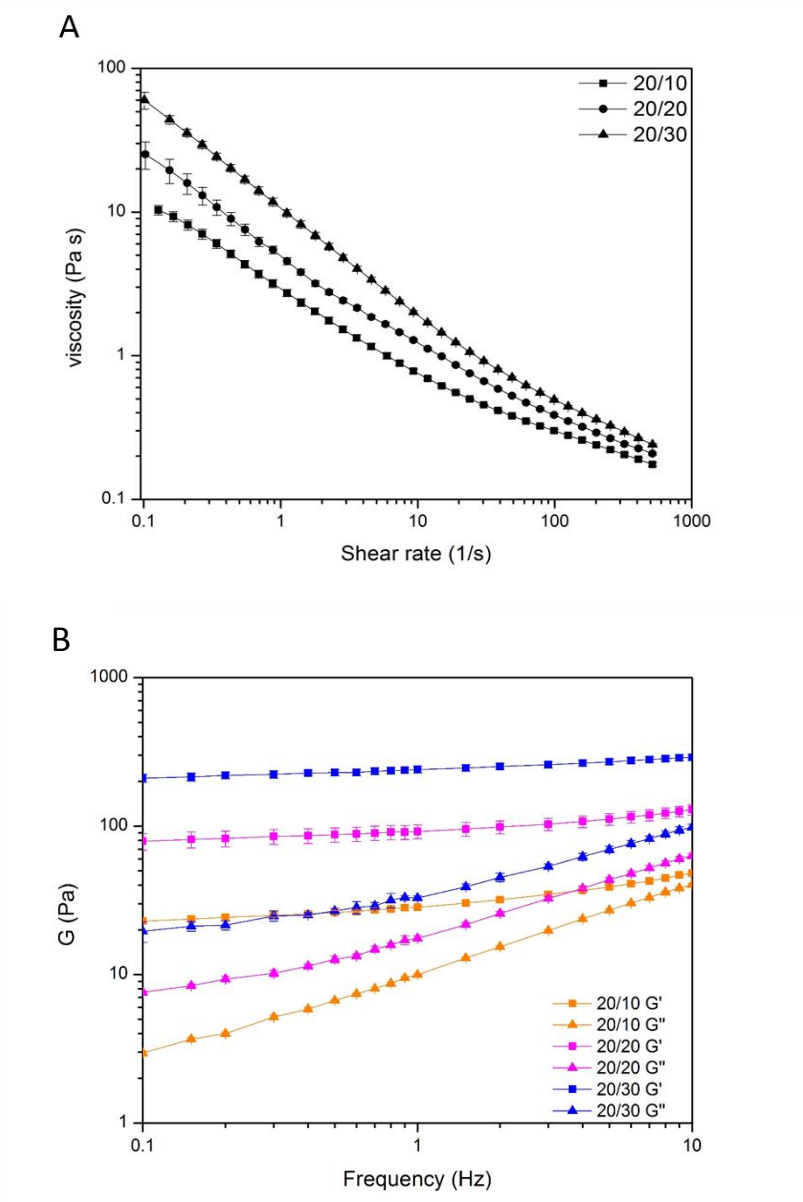

Figure S1. Rheological behavior of alginate bioinks. (A) Flow curves of three different bioink formulations, 20/10, 20/20, and 20/30. (B) Elastic modulus (G') and viscous modulus (G") of three different bioink formulations, 20/10, 20/20, and 20/30 as a function of frequency.

Appendix B: Supplementary date for characterization of hybrid hydrogel with cells

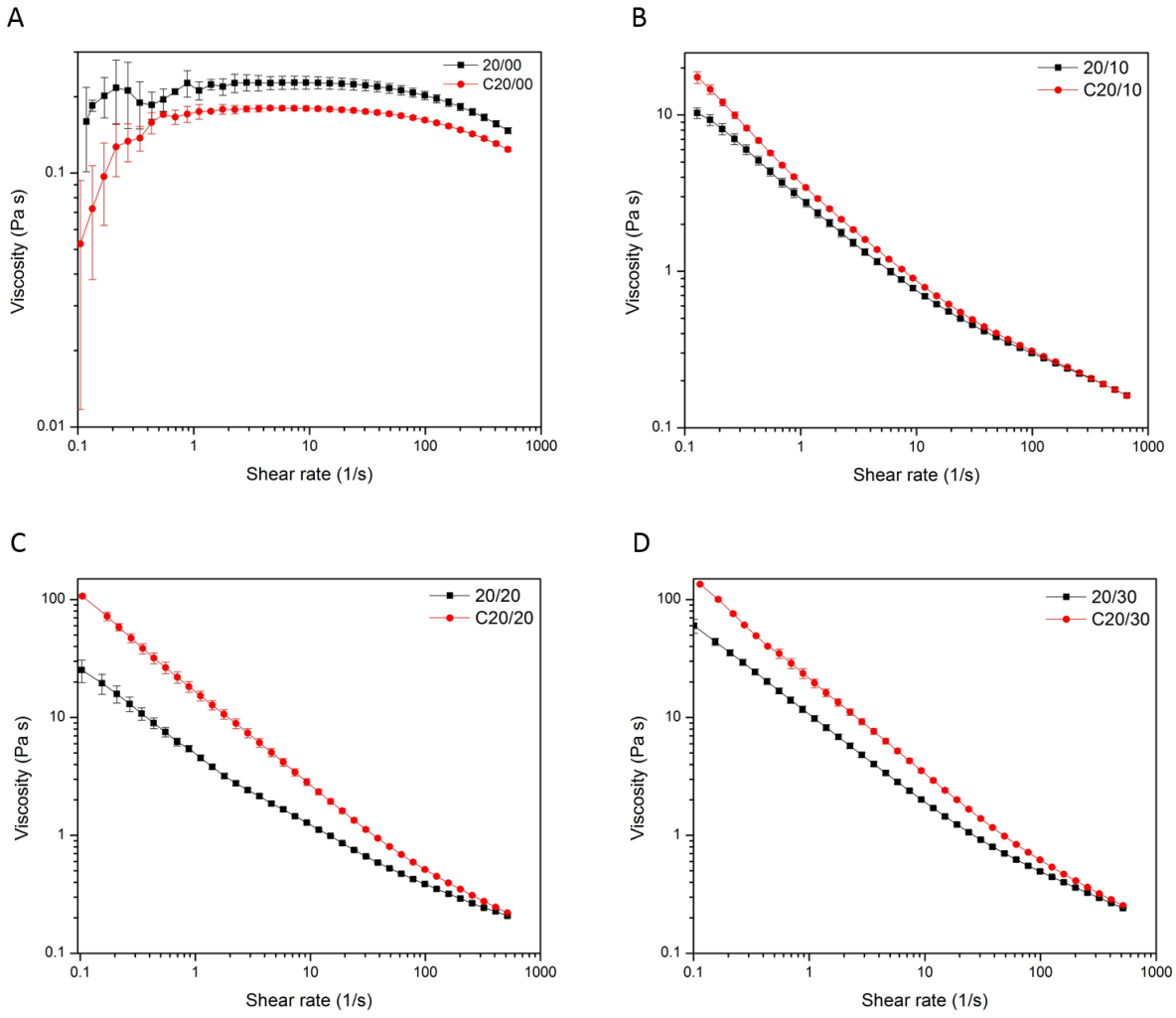

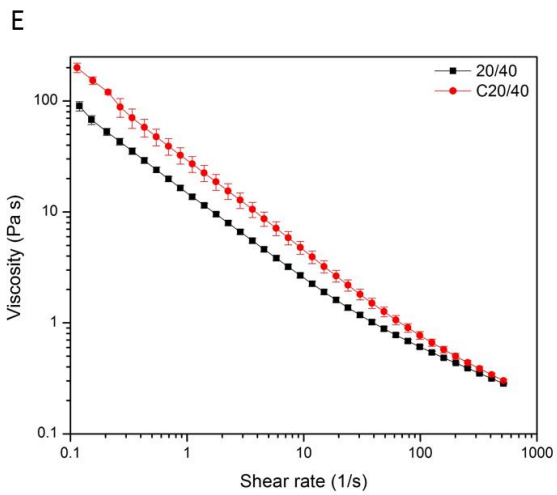

Figure S2. Flow curves of the five different bioink formulations with and without cells.